

# Deep Reinforcement Learning for Optimal Power Flow with Renewables Using Spatial-Temporal Graph Information

Jinhao Li, Ruichang Zhang, Hao Wang, *Member IEEE*,  
Zhi Liu, *Member IEEE*, Hongyang Lai, Yanru Zhang, *Member IEEE*

**Abstract**—Renewable energy resources (RERs) have been increasingly integrated into modern power systems, especially in large-scale distribution networks (DNs). In this paper, we propose a deep reinforcement learning (DRL)-based approach to dynamically search for the optimal operation point, i.e., optimal power flow (OPF), in DN with a high uptake of RERs. Considering uncertainties and voltage fluctuation issues caused by RERs, we formulate OPF into a multi-objective optimization (MOO) problem. To solve the MOO problem, we develop a novel DRL algorithm leveraging the graphical information of the distribution network. Specifically, we employ the state-of-the-art DRL algorithm, i.e., deep deterministic policy gradient (DDPG), to learn an optimal strategy for OPF. Since power flow reallocation in the DN is a consecutive process, where nodes are self-correlated and interrelated in temporal and spatial views, to make full use of DN's graphical information, we develop a multi-grained attention-based spatial-temporal graph convolution network (MG-ASTGCN) for spatial-temporal graph information extraction, preparing for its sequential DDPG. We validate our proposed DRL-based approach in modified IEEE 33, 69, and 118-bus radial distribution systems (RDSs) and show that our DRL-based approach outperforms other benchmark algorithms. Our experimental results also reveal that MG-ASTGCN can significantly accelerate the DDPG training process and improve DDPG's capability in reallocating power flow for OPF. The proposed DRL-based approach also promotes DN's stability in the presence of node faults, especially for large-scale DN.

**Index Terms**—Optimal power flow (OPF), renewable energy resources (RERs), deep reinforcement learning (DRL), graph convolution, attention mechanism.

## I. INTRODUCTION

THERE has been an exponential growth of distributed renewable energy resources (RERs) in the distribution networks (DNs) to deal with global climate change and cut customers' electricity bills. Both design and operation of power systems have gradually evolved towards a distributed manner instead of centralized management [1]. From the year 2007 to 2020, the global installed capacity of solar photovoltaic (PV) has increased from 8 Gigawatts (GW) to 760 GW, and the wind power capacity has also risen from 94 GW to 743 GW [2]. Although the adoption of RERs in conventional power systems offers various benefits, such as

decarbonizing the electricity market and reducing the energy supply costs, the integration of RERs into conventional power systems, at the same time, poses significant challenges due to their intermittent nature. [3].

A major challenge is that the stability of DN can be affected by the uncertainty introduced by RERs, and maintaining a stable and optimal operating point, i.e., the best working states for each node in DN, is always a top priority for power systems, which not only mitigates severe outages but also minimizes operating costs [4]. In power systems without renewables, the optimal operation point can be easily found since the operating state of each node and branch can be accurately predicted and the power output of each power generator is already scheduled [5]. However, the generation of RERs is unstable and uncontrollable, which can be affected by various external factors, such as solar irradiation and wind velocity for solar and wind power, respectively. Thus, the unstable nature of RERs leads to a consecutive change in the optimal operation point. Meanwhile, since both exact timing and the number of newly generated RERs cannot be predicted, the addition of RERs inevitably causes several technical issues, such as voltage fluctuation and harmonic distortion, which threaten the stability of DN and cause potential economic losses [6]. This paper takes these factors into consideration and aims to address the major challenge of how to adjust the optimal operation point, dynamically, rapidly, and effectively for DN when connected to RERs.

Calculating the optimal operation point in power systems is known as solving the optimal power flow (OPF) problem [7]. In the past decades, OPF has been extensively studied as an optimization problem whose objective is to minimize the cost of power generation while satisfying operating constraints and demands. Considering uncertainties and voltage fluctuation issues in DN with a high uptake of RERs, we formulate OPF into a multi-objective optimization problem (MOO) to reduce the impact of uncertainties and mitigate voltage fluctuation. The existing studies on solving OPF can be briefly categorized into three classes—typical numerical, heuristic, and deep-learning algorithms:

- *Typical numerical algorithms*: Typical numerical methods, such as the Gauss-Seidel and Newton-Raphson methods, have proved their excellent performance in conventional power systems [8]. However, the integration of RERs introduces uncertainties that complicate the highly nonlinear OPF problem, which makes these methods extremely difficult to converge.
- *Heuristic algorithms*: There has been increasing attention on adopting heuristic algorithms to solve the complex OPF problem [9]–[12]. However, these heuristics may be less effective when it comes to large-scale DN, as

Manuscript received April 19, 2021; revised August 16, 2021.

J. Li, H. Lai are with the School of Mechanical and Electrical Engineering, University of Electronic Science and Technology of China, Chengdu, China, 611731 (e-mail:jinhaoli@std.uestc.edu.cn, laihongyang0314@outlook.com).

R. Zhang, Y. Zhang are with the School of Computer Science and Engineering, University of Electronic Science and Technology of China, Chengdu, China, 611731 (e-mail:yanruzhang@uestc.edu.cn, zhangruichang2@gmail.com). Y. Zhang is the corresponding author.

H. Wang is with the Department of Data Science and Artificial Intelligence, Faculty of Information Technology, Monash University, Melbourne, VIC 3800, Australia (e-mail: hao.wang2@monash.edu).

Z. Liu is with Department of Computer and Network Engineering, University of Electro-Communications, Tokyo, Japan (e-mail:liu@ieec.org).

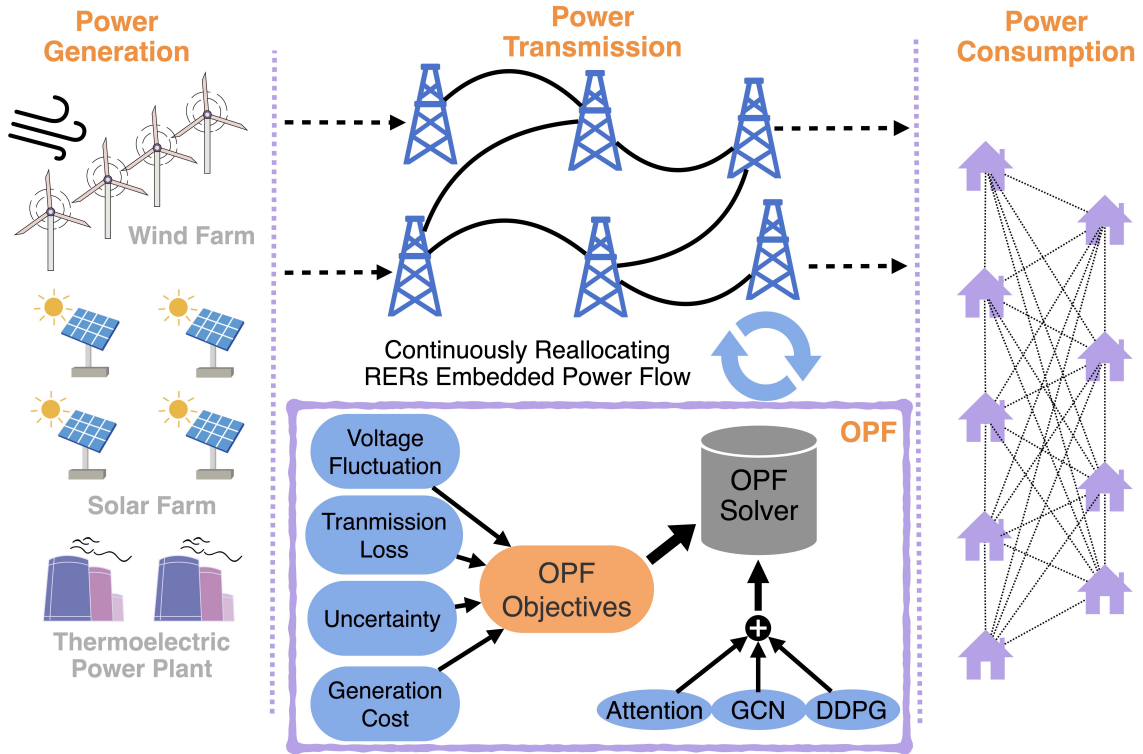


Fig. 1. The system model and the presented work.

most of these algorithms are model-based and highly dependent on accurate knowledge of DNs [13]. Besides, heuristic algorithms are sensitive to their initialization values. Meanwhile, heuristic algorithms suffer from a heavy computational burden and can trap into local optimum.

- *Deep-learning algorithms:* Recently, with the rapid emergence of artificial intelligence and particularly deep learning, a variety of data-driven methods based on deep learning have been introduced to solve OPF problems in DNs [13]–[15]. Indeed, these approaches require a large amount of historical data to train an accurate deep learning model. Therefore, it is inherently challenging for deep learning-based algorithms to react quickly in tracking dynamic best operating points, as these models need to re-collect a large amount of data once the newly generated RERs enter the DN.

To overcome the above drawbacks, this paper introduces deep reinforcement learning (DRL) to solve the OPF problem in DNs. DRL is known for its powerful capability in solving complex decision-making problems [16], [17], which can be perfectly adopted here to capture the dynamic features in RERs-embedded power flow reallocation process. The proposed DRL-based approach aims to learn gradually how to optimize power flow in DNs and dynamically find the optimal operating point, which can significantly mitigate the impact of uncertainties in DNs.

However, training a stable and well-performed DRL agent is time-consuming due to its slow convergence speed [16]. Indeed, an essential feature about power flow, namely its

spatial-temporal (ST) information, has been neglected in the aforementioned literature. In fact, RERs-embedded power flow reallocation can be considered as a consecutive process in which each node in the DN is self-correlated and interrelated in temporal and spatial views. Such ST information contains a prior knowledge of the DN graph, and can play a significant role for the DRL agent to search OPF more effectively. To accelerate the DRL algorithm’s convergence speed, we therefore introduce a multi-grained attention-based spatial-temporal convolution network (MG-ASTGCN) to extract ST correlations through attention mechanism [18] and ST features through graph convolution [19]–[21], providing sufficient auxiliary information for the sequential DRL-based approach. An overview of the presented work is illustrated in Fig. 1.

The main contributions of our work are summarized as follows.

- *Extraction of Spatial and Temporal Information:* MG-ASTGCN is introduced to fully extract ST information in dynamic power flow, where attention mechanism and graph convolution are adopted to mine ST correlations and features in spatial and temporal aspects, respectively. Additionally, considering that power flow may show periodic patterns in different time scales, we construct multi-grained power flow segments to capture different time-scaled ST information among historical power flow. Thus, MG-ASTGCN can provide global prior knowledge about current DN, and prepare for the sequential DDPG to conduct effective power flow adjustment.
- *Solving OPF by DRL:* A DRL-based approach is developed to solve the OPF problem with the high renewable

penetration in DNs. Our algorithm can dynamically adjust power flow to search for the optimal operation point and also quickly respond to uncertainties brought in by RERs. Specifically, the OPF problem is formulated into a Markov Decision Process (MDP). Then, the deep deterministic policy gradient (DDPG) algorithm is adopted to solve the derived MDP, which outperforms other DRL algorithms according to our experimental results.

The key insights drawn from our work are summarized as follows.

- *Impacts of Attention Mechanism in MG-ASTGCN*: The spatial attention mechanism in MG-ASTGCN aims to capture the correlation strengths among nodes in the DN, while temporal attention exploits temporal dependencies between current and historical power flow. Our experiments shows that node pairs in the DN with more generator access have stronger spatial correlations. In the temporal view, each node's features are highly self-correlated in the past 10 power flow reallocation intervals.
- *The DRL-based approach converges faster with the addition of MG-ASTGCN*: Our experimental results reveal that the addition of MG-ASTGCN in DDPG can significantly improve DDPG's convergence speed, compared with other correlation extraction methods, which demonstrates effectiveness of the MG-ASTGCN in capturing ST graphical information in the DN.
- *DN tends to work in the sub-optimal operation point if controlling voltage fluctuation is overemphasized*. The DRL-based approach encodes all operational constraints of the OPF problem into the reward functions as feedback from the DN itself. It is found that if the reward function for controlling voltage fluctuation is overemphasized, the performance of the DRL agent degenerates simultaneously, which results in sub-optimal operation of the DN.

The remainder of this paper is organized as follows. In Section II, the system model is presented. The MG-ASTGCN and DRL-based approach are introduced in Section III. The experimental setup and results are presented in Section IV. Section V concludes this paper.

## II. SYSTEM MODEL

Consider that there is a DN with conventional energy resources, wind power, and solar PV power. We use wind and solar PV power to represent RERs, since they are the most representative RERs in DNs with the largest installed capacities [2]. In this section, we first introduce the basic formulation of the OPF problem without RERs. The integration of RERs introduces uncertainties to DNs and leads to the voltage fluctuation issue, which results in a more complicated OPF problem. Then, OPF is reformulated, in which both the uncertainty factors from wind and solar PV power and voltage fluctuation control are considered.

### A. OPF Formulation with Conventional Energy Resources Only

OPF with conventional energy resources can be considered as a single-objective optimization (SOO) problem. Its objective

function is to minimize the cost of power generation while still satisfying physical constraints of the DN at each power flow reallocation interval, which can be formulated as:

$$J_{\text{soo}}(P_t) = \sum_{i=1}^{N_t} C_t(P_{t,i}), \quad (1)$$

where  $N_t$  is the total number of thermoelectric generators,  $P_{t,i}$  is the active power output of the  $i$ th thermoelectric generator, and  $C_t(\cdot)$  is the corresponding energy generation cost function which is defined as a quadratic polynomial [22]:

$$C_t(P_{t,i}) = a_i(P_{t,i})^2 + b_i P_{t,i} + c_i, \quad (2)$$

where  $a_i$ ,  $b_i$ , and  $c_i$  are coefficients of the  $i$ th thermoelectric generator's cost function.

Considering the valve-point effect, which can be modeled as a sinusoidal function [23], Eq. (2) can be reformulated as:

$$C_t(P_{t,i}) = a_i(P_{t,i})^2 + b_i P_{t,i} + c_i + |d_i \sin(e_i(P_{t,i} - P_{t,i}^{\min}))|, \quad (3)$$

where  $d_i$  and  $e_i$  are coefficients associated with the valve-point effect, and  $P_{t,i}^{\min}$  is the minimum power output by the  $i$ th thermoelectric generator.

### B. OPF Formulation with Renewable Energy Resources

With a high uptake of wind and solar PV power, both uncertainties and the voltage fluctuation issue threaten the DN's stability. To stabilize nodes' voltages and mitigate the uncertainty, we can transform the original SOO problem defined in Eq. (1) into a multi-objective optimization for OPF (MOO-OPF). We describe these details in detail below.

1) *Direct Cost of Wind and Solar PV Power Generation*: The direct cost of wind power generated by the  $j$ th wind power turbine can be characterized as a function of the scheduled power output:

$$C_{w,j}^d(P_{w,j}) = f_j P_{w,j}, \quad (4)$$

where  $C_{w,j}^d(\cdot)$  is the direct cost function of the  $j$ th wind power turbine,  $f_j$  is the coefficient of the  $j$ th wind power turbine's cost function, and  $P_{w,j}$  is the scheduled wind power output from  $j$ th wind power turbine.

Similarly, the direct cost of solar PV power generators can be formulated as:

$$C_{s,k}^d(P_{s,k}) = g_k P_{s,k}, \quad (5)$$

where  $C_{s,k}^d(\cdot)$  is the direct cost function of the  $k$ th solar PV power generator,  $g_k$  is the coefficient of  $k$ th solar PV power generator's cost function, and  $P_{s,k}$  is the scheduled solar PV power output from  $k$ th solar PV power generator [24].

#### 2) *Uncertainties Cost of Wind Power*:

**Reserve Cost of Wind Power:** There is a common scenario in DN that the amount of generated wind power is lower than its corresponding scheduled one, which is termed as power overestimation from the uncertain source [25]. The spinning of wind power turbines should be reserved to deliver uninterrupted supply to consumers under this circumstance,

whose corresponding cost is defined as the reserve cost, which can be formulated as:

$$\begin{aligned} C_{w,j}^r (P_{w,j} - P_{w,j}^a) &= h_{w,j}^r (P_{w,j} - P_{w,j}^a) \\ &= h_{w,j}^r \int_0^{P_{w,j}} (P_{w,j} - p_{w,j}) f_w(p_{w,j}) d(p_{w,j}), \end{aligned} \quad (6)$$

where  $C_{w,j}^r(\cdot)$  is the reserve cost function of the  $j$ th wind power turbine,  $h_{w,j}^r$  is the coefficient corresponding to the  $j$ th wind power turbine's reserve cost,  $P_{w,j}^a$  is the available power that can be reallocated from  $j$ th wind power turbine,  $p_{w,j}$  is the integration variable in interval  $(0, P_{w,j})$ , and  $f_w(p_{w,j})$  is the wind power probability density function (PDF) of the  $j$ th wind power turbine. The details about calculating wind power PDF is presented in Section II-C1.

**Penalty Cost of Wind Power:** The above overestimation scenario can be reversed when power outputs of wind power turbines are higher than their scheduled ones, which is known as power underestimation from the uncertain source. Under this underestimation scenario, if there is no way to reduce power generation from thermoelectric generators, the redundant power provided by wind power turbines will be abandoned. Hence, its corresponding cost is expressed as the penalty cost, which can be formulated as:

$$\begin{aligned} C_{w,j}^p (P_{w,j}^a - P_{w,j}) &= h_{w,j}^p (P_{w,j}^a - P_{w,j}) \\ &= h_{w,j}^p \int_{P_{w,j}}^{P_{w,j}^a} (p_{w,j} - P_{w,j}) f_w(p_{w,j}) d(p_{w,j}), \end{aligned} \quad (7)$$

where  $C_{w,j}^p(\cdot)$  is the penalty cost function of the  $j$ th wind power turbine,  $h_{w,j}^p$  is the coefficient related to the  $j$ th wind power turbine's penalty cost, and  $P_{w,j}^r$  is the rated power output of the  $j$ th wind power turbine.

3) *Uncertainties Cost of Solar PV Power:* In general, the uncertainty cost of solar PV power can be calculated in a similar way to that of wind power [26].

**Reserve Cost of Solar PV Power:** The reserve cost of the  $k$ th solar PV power generator is formulated as:

$$\begin{aligned} C_{s,k}^r (P_{s,k} - P_{s,k}^a) &= h_{s,k}^r (P_{s,k} - P_{s,k}^a) \\ &= h_{s,k}^r f_s(P_{s,k}^a < P_{s,k}) [P_{s,k} - \mathbb{E}(P_{s,k}^a < P_{s,k})], \end{aligned} \quad (8)$$

where  $C_{s,k}^r(\cdot)$  is the reserve cost function of the  $k$ th solar PV power generator,  $h_{s,k}^r$  is the coefficient corresponding to the  $k$ th solar PV power generator's reserve cost,  $P_{s,k}^a$  is the available power that can be reallocated from  $k$ th solar PV power generator,  $f_s(P_{s,k}^a < P_{s,k})$  represents the probability of solar PV power shortage, and  $\mathbb{E}(P_{s,k}^a < P_{s,k})$  is the expectation of solar PV power for solar PV power shortage occurrence.

Similarly, the penalty cost of the  $k$ th solar PV generator is expressed as the reverse form of Eq. (8):

$$\begin{aligned} C_{s,k}^p (P_{s,k}^a - P_{s,k}) &= h_{s,k}^p (P_{s,k}^a - P_{s,k}) \\ &= h_{s,k}^p f_s(P_{s,k}^a > P_{s,k}) [\mathbb{E}(P_{s,k}^a > P_{s,k}) - P_{s,k}], \end{aligned} \quad (9)$$

4) *Voltage Fluctuation Control in MOO-OPF:* Due to the intermittent nature of RERs, voltage fluctuation can occur in the DN when connected to RERs, which degrades the performance of electronic equipment and poses potential security risks on residential, commercial, and industrial power

consumers. To mitigate the effect of voltage fluctuation into a tolerant range, minimizing the voltage fluctuation is represented as the second objective in the MOO-OPF problem. To better describe the temporal correlation of voltages, since each node's voltage may increase or decrease rapidly in several neighboring intervals, the objective function is expressed as a temporal difference (TD) form:

$$F^v = \sum_{j=1}^{N_t + N_l} \left| V_j^{t_0} - \frac{1}{T_{td}} \sum_{t=1}^{T_{td}} V_j^{t_0 - t} \right|, \quad (10)$$

where  $N_t$  and  $N_l$  are the total number of thermoelectric generators and buses, respectively,  $V_j^{t_0}$  is  $j$ th bus voltages at  $t_0$  power reallocation intervals. To better capture the historical voltage information, one-step TD method is adapted to the multi-step TD in Eq. (10) with a multi-step parameter  $T_{td}$ .

5) *Transmission Loss in MOO-OPF:* Transmitting power to consumers inevitably leads to power losses in any power systems, which can be formulated as:

$$P^l = \sum_{b=1}^{N_b} G_{i,j} [V_i^2 + V_j^2 - 2V_i V_j \cos(\delta_{ij})], \quad (11)$$

where  $N_b$  is the total number of branches in DN,  $\delta_{ij} = \delta_i - \delta_j$  represents the voltage angle difference between the  $i$ th and  $j$ th buses, and  $G_{i,j}$  is the transfer conductance of the  $b$ th branch connecting the  $i$ th and  $j$ th buses.

6) *Objective Functions of MOO-OPF:* There are three objective functions to minimize in the MOO-OPF problem:

#### Power generation cost

$$\begin{aligned} \min \sum_{i=1}^{N_t} C_t(P_{t,i}) &+ \sum_{j=1}^{N_w} [C_{w,j}^d(\cdot) + C_{w,j}^r(\cdot) + C_{w,j}^p(\cdot)] \\ &+ \sum_{k=1}^{N_s} [C_{s,k}^d(\cdot) + C_{s,k}^r(\cdot) + C_{s,k}^p(\cdot)]. \end{aligned} \quad (12)$$

#### Mitigating Voltage Fluctuation

$$\min F^v. \quad (13)$$

#### Power Transmission Loss

$$\min P^l. \quad (14)$$

7) *Constraints of MOO-OPF:* Objectives of the MOO-OPF problem described in Eq. (12) to (14) are subject to physical constraints that ensure the proper operation of power systems and can be divided into equality constraints and inequality constraints [24].

**Equality Constraints:** Both generated active power and reactive power must be equal to power demand and power losses in power systems, named power balance, which can be formulated as:

$$P_{gi} - P_{li} = V_i \sum_{b=1}^{N_b} V_j (G_{i,j} \cos \delta_{ij} + B_{i,j} \sin \delta_{ij}), \quad (15)$$

$$Q_{gi} - Q_{li} = V_i \sum_{b=1}^{N_b} V_j (G_{i,j} \sin \delta_{ij} + B_{i,j} \cos \delta_{ij}), \quad (16)$$



where  $P_{li}$  and  $Q_{li}$  represent the active and reactive power of the  $i$ th bus, respectively,  $P_{gi}$  and  $Q_{gi}$  are the active and reactive power generated from generators at the  $i$ th bus, respectively, and  $Y_{i,j} = G_{i,j} + jB_{i,j}$  the admittance between the  $i$ th and  $j$ th buses [27].

### Inequality Constraints:

$$\underline{P}_{t,i} \leq P_{t,i} \leq \bar{P}_{t,i}, \quad i = 1, \dots, N_t, \quad (17)$$

$$\underline{P}_{w,j} \leq P_{w,j} \leq \bar{P}_{w,j}, \quad j = 1, \dots, N_w, \quad (18)$$

$$\underline{P}_{s,k} \leq P_{s,k} \leq \bar{P}_{s,k}, \quad k = 1, \dots, N_s, \quad (19)$$

$$\underline{Q}_{t,i} \leq Q_{t,i} \leq \bar{Q}_{t,i}, \quad i = 1, \dots, N_t, \quad (20)$$

$$\underline{Q}_{w,j} \leq Q_{w,j} \leq \bar{Q}_{w,j}, \quad j = 1, \dots, N_w, \quad (21)$$

$$\underline{Q}_{s,k} \leq Q_{s,k} \leq \bar{Q}_{s,k}, \quad k = 1, \dots, N_s, \quad (22)$$

$$\underline{V}_{t,i} \leq |V_{t,i}| \leq \bar{V}_{t,i}, \quad i = 1, \dots, N_t, \quad (23)$$

$$\underline{V}_{w,j} \leq |V_{w,j}| \leq \bar{V}_{w,j}, \quad j = 1, \dots, N_w, \quad (24)$$

$$\underline{V}_{s,k} \leq |V_{s,k}| \leq \bar{V}_{s,k}, \quad k = 1, \dots, N_s, \quad (25)$$

$$\underline{V}_{l,p} \leq |V_{l,p}| \leq \bar{V}_{l,p}, \quad p = 1, \dots, N_l, \quad (26)$$

$$|S_b| \leq \bar{S}_b, \quad b = 1, \dots, N_b, \quad (27)$$

where  $\underline{P}$  and  $\bar{P}$ ,  $\underline{Q}$  and  $\bar{Q}$ ,  $\underline{V}$  and  $\bar{V}$  represent their corresponding minimum and maximum values, respectively.

In the above inequality constraints, Eq. (17) to (25) are generator constraints, where Eq. (17) to (19) describe the active power generation limits of thermoelectric generators, wind power turbines, and solar PV generators. Eq. (20) to (22) and Eq. (23) to (25) illustrate the reactive power capabilities and voltage limits of their corresponding generators, respectively. Constraints from Eq. (26) to (27) restrict bus capacities and line capacities in a tolerant range. Note that voltage of each node, take  $\mathbb{V}_{t,i} = V_{t,i} \angle \delta_{t,i}$  as an example, is a complex number, containing its voltage amplitude  $V_{t,i}$  as the real part and its voltage angle  $\delta_{t,i}$  as the imaginary part. Similarly, apparent power on each branch  $\mathbb{S}_b$  is also a complex number, in which  $P_{i,j}$  and  $Q_{i,j}$  represent its real and imaginary parts, respectively.

### C. Uncertainty Models of Wind and Solar PV Power

Both wind and solar PV power are random variables due to their intermittent nature. We develop two stochastic models to figure out the uncertainties cost, i.e., reserve costs and penalty costs defined from Eq. (6) to (7) and Eq. (8) to (9).

1) *Stochastic Wind Power Model*: The wind velocity distribution has been proven to follow the Weibull PDF through extensive studies [25], [28], which can be formulated as:

$$f(v) = \frac{k}{c} \left(\frac{v}{c}\right)^{k-1} \exp\left[-\left(\frac{v}{c}\right)^k\right], \quad \forall v \in (0, \infty), \quad (28)$$

where  $k$  and  $c$  represent the shape and scale factors, respectively, and the expectation of wind speed can be expressed as:

$$\mathbb{E}_{v \sim f(v)}(v) = c\Gamma(v)(1 + k^{-1}), \quad (29)$$

where the gamma function  $\Gamma(v)$  can be formulated as:

$$\Gamma(v) = \int_0^\infty e^{-t} t^{v-1} dt. \quad (30)$$

The actual power output from a wind turbine relies on the wind speed it encounters, which can be expressed as:

$$p_w(v) = \begin{cases} 0, & v \in (0, v^{\text{in}}) \cup (v^{\text{out}}, \infty), \\ p_w^r \cdot \frac{v - v^{\text{in}}}{v^r - v^{\text{in}}}, & v \in [v^{\text{in}}, v^r], \\ p_w^r, & v \in (v^r, v^{\text{out}}], \end{cases} \quad (31)$$

where  $v^{\text{in}}$ ,  $v^{\text{out}}$ , and  $v^r$  are the cut-in, cut-out, and rated wind speeds of a wind turbine, respectively, and  $p_w^r$  is the rated power output of a wind turbine.

Based on Eq. (31), the probabilities of different wind power outputs can be calculated as:

$$f(p_w) = \begin{cases} 1 - \exp\left[-\left(\frac{v^{\text{in}}}{c}\right)^k\right] + \exp\left[-\left(\frac{v^{\text{out}}}{c}\right)^k\right], \\ \frac{k(v^r - v^{\text{in}})}{c^k p_w^r} \left[v^{\text{in}} + \frac{p_w}{p_w^r}(v^r - v^{\text{in}})\right]^{k-1} \cdot \gamma^d, \\ \exp\left[-\left(\frac{v^r}{c}\right)^k\right] - \exp\left[-\left(\frac{v^{\text{out}}}{c}\right)^k\right], \end{cases} \quad (32)$$

where the above formulas are corresponded with different power output circumstances presented in Eq. (31), and  $\gamma^d$  represents the exponential decay term, which can be formulated as:

$$\gamma^d = \exp\left\{-\frac{\left[v^{\text{in}} + \frac{p_w}{p_w^r}(v^r - v^{\text{in}})\right]^k}{c^k}\right\}. \quad (33)$$

2) *Stochastic Solar PV Power Model*: The intermittent nature of solar PV power is determined by solar irradiance  $G$  which follows the lognormal PDF [29]. The probability of solar irradiance can be defined as:

$$f(G) = \frac{1}{G\sigma\sqrt{2\pi}} \exp\left[-\frac{(\ln G - \mu)^2}{2\sigma^2}\right], \quad \forall G > 0, \quad (34)$$

where  $\mu$  and  $\sigma$  are the expected value and standard deviation of  $G$ 's natural logarithm, and the expectation of  $G$  can be calculated as:

$$\mathbb{E}_{G \sim f(G)}(G) = \exp\left(\mu + \frac{\sigma^2}{2}\right). \quad (35)$$

The conversion process from solar irradiance to solar PV power via a solar PV generator is expressed as [30]:

$$P_s(G) = \begin{cases} P_s^r \cdot \frac{G^2}{G^{\text{std}} R_c}, & G \in (0, R_c), \\ P_s^r \cdot \frac{G}{G^{\text{std}}}, & G \in [R_c, \infty), \end{cases} \quad (36)$$

where  $P_s^r$  is the rated power output of a solar PV generator,  $G^{\text{std}}$  represents solar irradiance in a standard environment, and  $R_c$  is a certain solar irradiance point.

## III. METHODOLOGY

In this section, we propose a DRL-based approach to solve the complicated MOO-OPF problem described from Eq. (12) to (13), in which the MOO-OPF is first abstracted to a markov decision process (MDP). Among the variety of DRL algorithms, DDPG is adopted to solve the MDP, which shows its outstanding performance compared to others. Additionally, the MG-ASTGCN is introduced to fully extract ST information in DN, which helps the sequential DDPG for better decision making.

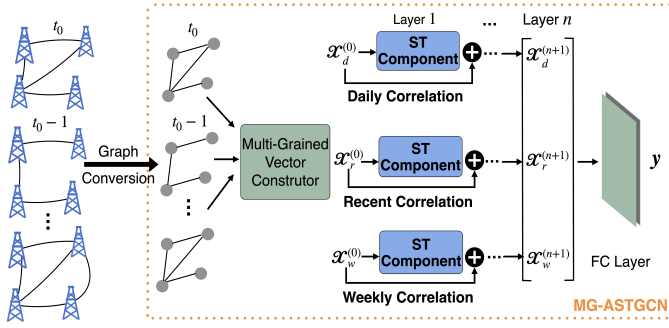


Fig. 2. The framework of the proposed MG-ASTGCN. Firstly, DN at different power flow reallocation intervals are transformed into a series of graphs. Then, multiple time-scaled segments, i.e., the recent, daily, and weekly segments, are constructed from these derived graphs for spatial-temporal information extraction. In the end, FC layer process the outputs of the three segments and outputs the final spatial-temporal information vector for the sequential DDPG.

### A. Spatial-Temporal Correlations Extraction via MG-ASTGCN

To better exploit ST statistical properties of power flow, which has shown non-linearities and complex patterns with the high penetration of RERs, we develop the MG-ASTGCN, which combines graph convolution and attention mechanism [18], [19], [21], [31]–[33], to capture ST features and correlations among nodes in DN.

1) *Preliminaries of MG-ASTGCN*: DN can be transformed into an undirected graph  $\mathcal{G} = (\mathcal{V}, \mathcal{E}, \mathbf{A})$  as illustrated in Fig. 3.  $\mathcal{V}$  is a finite set of  $|\mathcal{V}| = N$  nodes where  $N = N_t + N_w + N_s + N_l$ . More precisely,  $\mathcal{V}$  includes all generators and buses in DN.  $\mathcal{E}$  is a finite set of edges that indicates all branches in DN.  $\mathbf{A} \in \mathbb{R}^{N \times N}$  represents the adjacency matrix of graph  $\mathcal{G}$ . Each node  $v_i$  in  $\mathcal{V}$  generates a feature vector  $\mathbf{x}_i \in \mathbb{R}^{F_i \times 1}$  at any power flow reallocation interval, including the  $i$ th node active power  $P_i$ , reactive power  $Q_i$ , voltage  $\mathbb{V}_i = V_i \angle \delta_i$ , and all branches' power related to the  $i$ th node  $\mathbb{S}_{i,j} = P_{i,j} + jQ_{i,j}$ . The feature vector of the  $i$ th node can be formulated as:

$$\mathbf{x}_i = (P_i, Q_i, \mathbb{V}_i, \mathbb{S}_{i,j_1}, \mathbb{S}_{i,j_2}, \dots)^T \in \mathbb{R}^{F_i \times 1}, \quad (37)$$

where  $F_i$  represents the number of features at the  $i$ th node.

The feature vector  $\mathbf{x}_i$  perfectly gathers local stationary information of the  $i$ th node and prepares for further ST correlation mining and feature extraction in Section III-A2 and III-A3.

The feature vector of DN  $\mathbf{X}$  can be calculated by concatenating each node's feature vector, which can be expressed as:

$$\mathbf{X} = (\mathbf{x}_1, \mathbf{x}_2, \dots, \mathbf{x}_N) \in \mathbb{R}^{N \times F}, \quad (38)$$

where  $F$  is the maximum number of features in which  $F = \arg \max_{F_i} \mathbf{x}_i$ .

The structure of DN graph changes dynamically after every power flow reallocation since both nodes' features and branches' power are already adjusted. Based on the assumption of the existence of periodic patterns in the power flow [2], a multi-grained vector constructor is introduced to better capture temporal correlations of a series of  $\mathcal{G}$ s, as shown in Fig. 2, which divides the  $\mathcal{G}$ s into three segments in the temporal dimension:

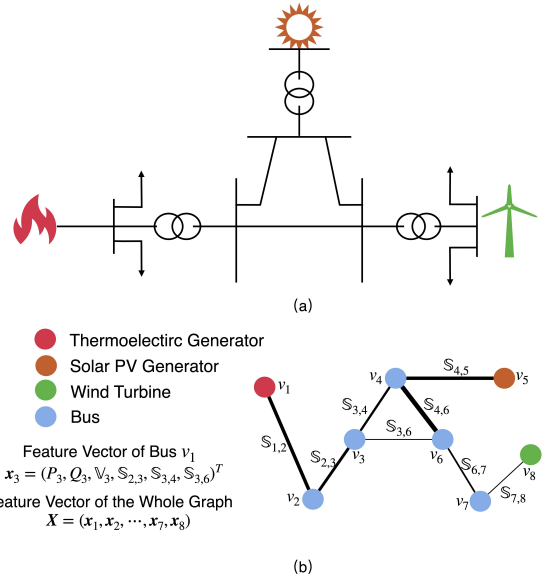


Fig. 3. An example of transforming DN into a graph. (a) represents a simplified example of DN diagram, including both conventional energy and RERs generation. The diagram is transformed into an undirected graph  $\mathcal{G} = (\mathcal{V}, \mathcal{E}, \mathbf{A})$  in (b), where the thickness of edges indicates different power flow  $\mathbb{S}$  on these branches. Note that the graph in (b) changes dynamically, since features on both nodes and edges are influenced by power flow reallocation at each interval.

- Recent segment  $\mathcal{X}_r \in \mathbb{R}^{F \times N \times T_s}$ ,

$$\mathcal{X}_r = \{\mathbf{X}_{t_0 - T_s + 1}, \dots, \mathbf{X}_{t_0 - 1}, \mathbf{X}_{t_0}\}, \quad (39)$$

where  $t_0$  is denoted as the current power flow reallocation interval, and  $T_s$  represents the length of recent segment along time axis. To maintain DN's stability, power flow reallocation process conducts gradually. Thus, it is reasonable to take into account the most recent graph vectors.

- Daily segment  $\mathcal{X}_d \in \mathbb{R}^{F \times N \times T_d}$ ,

$$\mathcal{X}_d = \{\mathbf{X}_{t_0 - T_d \times n_{rd}}, \dots, \mathbf{X}_{t_0 - n_{rd}}, \mathbf{X}_{t_0}\}, \quad (40)$$

where  $T_d$  is the length of daily segment along time axis. Assume that the DN operator reallocates the power flow  $n_{rd}$  times per day. It is known that there are peak, off-peak, and regular electricity usages every day [34], [35]. Hence, the daily segment is constructed to capture daily patterns of power flow.

- Weekly segment  $\mathcal{X}_w \in \mathbb{R}^{F \times N \times T_w}$ ,

$$\mathcal{X}_w = \{\mathbf{X}_{t_0 - 7 \times T_w \times n_{rd}}, \dots, \mathbf{X}_{t_0 - 7 \times n_{rd}}, \mathbf{X}_{t_0}\}, \quad (41)$$

where  $T_w$  is the length of weekly segment along time axis. The reason for considering the long-term correlations is that the work of [36] and [37] have found that electricity usage shows weekly patterns periodically in one certain period.

The framework of the proposed MG-ASTGCN is illustrated in Fig. 2, including graph transformation operation, multi-grained vector constructor, and ASTGCN. ASTGCN is introduced to take the multi-grained segments defined from Eq. (39) to (41) as inputs, in which each segment passes through several

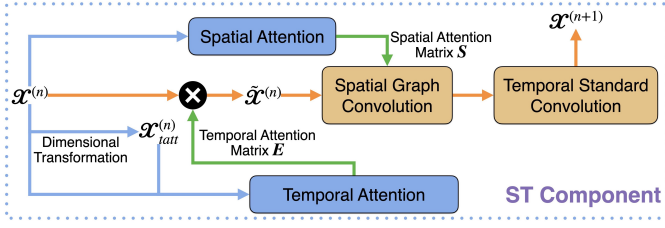


Fig. 4. The structure of one ST component.  $\mathcal{X}^{(n)}$  is the output of the previous ST component while  $\mathcal{X}^{n+1}$  represents the input for the next ST component.  $\mathcal{X}^{(n)}$ , together with the transformed  $\mathcal{X}_{tatt}^{(n)}$  is the input for the temporal attention mechanism.

ST components for ST information extraction. The structure of one ST component is presented in Fig. 4, including four major components: spatial attention, temporal attention, spatial graph convolution, and temporal standard convolution.

2) *Spatial-Temporal Attention Mechanism*: The ST attention mechanism is conducted before graph convolution, aiming to pay more attention to valuable graphical information in both spatial and temporal views on a series of DN graphs for the sequential convolution operations, which can be considered as a graph input preprocessing.

**Spatial Attention**: Since each two nodes in DN are connected by one transmission line practically, a slight fluctuation of one node's state, i.e., feature vector, may have an impact on its adjacent nodes. With the consecutive power flow reallocation, their mutual influence also changes dynamically. Hence, an attention mechanism in spatial dimension is needed to capture the dynamic correlations among nodes.

The spatial attention is formulated as:

$$\mathbf{S} = \mathbf{V}_s \odot \sigma \left( (\mathcal{X}^{n-1} \mathbf{W}_t)^T \mathbf{W}_{qk} (\mathbf{W}_f \mathcal{X}^{n-1})^T + \mathbf{b}_s \right), \quad (42)$$

where  $\mathbf{S} \in \mathbb{R}^{N \times N}$  represents the spatial attention matrix,  $\odot$  denotes the element-wise multiplication operation,  $\mathbf{V}_s, \mathbf{b}_s \in \mathbb{R}^{N \times N}$ ,  $\mathbf{W}_t \in \mathbb{R}^{T^{n-1}}$ ,  $\mathbf{W}_{qk} \in \mathbb{R}^{F^{n-1} \times T^{n-1}}$ , and  $\mathbf{W}_f \in \mathbb{R}^{F^{n-1}}$  are learnable parameters, the sigmoid function  $\sigma(\cdot)$  is adopted as activation function, and  $\mathcal{X}^{n-1} \in \mathbb{R}^{N \times F^{n-1} \times T^{n-1}}$  is the input of the  $n$ th ST component, which can be defined as:

$$\mathcal{X}^{n-1} = (\mathbf{X}_1, \mathbf{X}_2, \dots, \mathbf{X}_{T^{n-1}}), \quad (43)$$

where  $F^{n-1}$  and  $T^{n-1}$  represents the number of features and length of the temporal dimension after previous ST component processing, respectively, i.e.,  $F^{(0)} = F$  and  $T^{(0)} = T_s$  when the first ST component takes the original recent segment  $\mathcal{X}_r$  as input, and  $T^{(0)} = T_d$  and  $T^{(0)} = T_w$  for the original daily segment  $\mathcal{X}_d$  and weekly segment  $\mathcal{X}_w$ , respectively [20]. Obviously, the last two dimensions of  $\mathcal{X}$ , i.e.,  $F$  and  $T$ , change as it goes through multiple ST components since filters used in convolution have different sizes.

The definition of spatial attention mechanism in Eq. (42) is different from the typical attention formulation in [18], since the typical attention mechanism mostly applies to two-dimensional inputs, not to our three-dimensional segment. Spatial attention mechanism in this work aims to extract nodes' correlations topologically, the temporal dimension  $T_r$ ,

$T_d$ , and  $T_w$  can be eliminated after matrix multiplication between  $\mathcal{X}^{n-1}$  and  $\mathbf{W}_t$ . Similarly, our spatial attention focuses on correlations among nodes, which contains both local and global graphical information, instead of only one particular node's features. Thus, the feature dimension  $F$  is also removed by the same multiplication operation between  $\mathbf{W}_f$  and  $\mathcal{X}^{n-1}$ . Additionally, the learnable matrix  $\mathbf{W}_{qk}$  can connect the two matrices after dimension elimination and compute spatial correlations among nodes.  $\mathbf{V}_s$  is similar to the weighted value matrix in the typical attention mechanism, whose elements can be all initialized to 1.

Note that the value of element  $s_{i,j}$  in  $\mathbf{S}$ , named attention weight, semantically describes the correlation strength between the  $i$ th and  $j$ th nodes. Softmax operation is applied to ensure that the summation of attention weights related to each node is 1, which can be formulated as [38]:

$$\mathbf{S}'_{i,j} = \frac{\exp(\mathbf{S}_{i,j})}{\sum_{j=1}^N \exp(\mathbf{S}_{i,j})}. \quad (44)$$

When it comes to conducting graph convolution in Section III-A3, the normalized spatial attention matrix  $\mathbf{S}'$  is accompanied with the adjacency matrix  $\mathbf{A}$  to adjust attention weights among nodes.

**Temporal Attention**: Since DN operator needs to determine the amount of reallocated power flow based on each node's historical states, it is essential to track the temporal correlations of every node's state. Similar to the previous spatial attention, the temporal attention mechanism can be formulated as:

$$\mathbf{E} = \mathbf{V}_e \odot \sigma \left( (\mathbf{U}_n \mathcal{X}_{tatt}^{n-1})^T \mathbf{U}_{qk} (\mathbf{U}_f \mathcal{X}^{n-1}) + \mathbf{b}_e \right),$$

$$\mathbf{E}'_{i,j} = \frac{\exp(\mathbf{E}_{i,j})}{\sum_{j=1}^{T^{n-1}} \exp(\mathbf{E}_{i,j})} \in \mathbb{R}^{T^{n-1} \times T^{n-1}}, \quad (45)$$

where  $\mathbf{U}_f \in \mathbb{R}^{F^{n-1}}$ ,  $\mathbf{U}_n \in \mathbb{R}^N$ ,  $\mathbf{U}_{qk} \in \mathbb{R}^{F^{n-1} \times N}$ , and  $\mathbf{V}_e, \mathbf{b}_e \in \mathbb{R}^{T^{n-1} \times T^{n-1}}$  are all learnable parameters.  $\mathcal{X}_{tatt}^{n-1} \in \mathbb{R}^{N \times F^{n-1} \times T^{n-1}}$  is obtained by conducting matrix transpose operation on each graph vector of  $\mathcal{X}^{n-1}$ , which can be expressed as:

$$\mathcal{X}_{tatt}^{n-1} = (\mathbf{X}_1^T, \mathbf{X}_2^T, \dots, \mathbf{X}_{T^{n-1}}^T). \quad (46)$$

Similarly, our temporal attention mechanism aims to figure out each node's self-correlations in a series of DN graphs. Thus, it only focuses on the temporal dimension, where both the feature dimension  $F$  and spatial dimension  $N$  can be eliminated by using the two learnable matrices  $\mathbf{U}_n$  and  $\mathbf{U}_f$  to conduct the matrix multiplication.

$\mathbf{E}'$  is the normalized temporal attention matrix. Its element  $e'_{i,j}$  represents the strength of temporal dependency between two graph feature vectors  $\mathbf{X}_{t_0-i}$  and  $\mathbf{X}_{t_0-j}$ , which are generated at power flow reallocation intervals  $t_0 - i$  and  $t_0 - j$  in segment  $\mathcal{X}^{n-1}$ , respectively.  $\mathbf{U}_{qk}$  is used for calculating the temporal correlations of power flow reallocation intervals.

Since the temporal attention matrix directly describes the temporal dependencies of the given  $\mathcal{X}^{n-1}$ , the adjusted input for the sequential convolution operations  $\tilde{\mathcal{X}}^{n-1}$  can be obtained via matrix multiplication operation, expressed as:

$$\tilde{\mathcal{X}}^{n-1} = \mathcal{X}^{n-1} \mathbf{E}'. \quad (47)$$

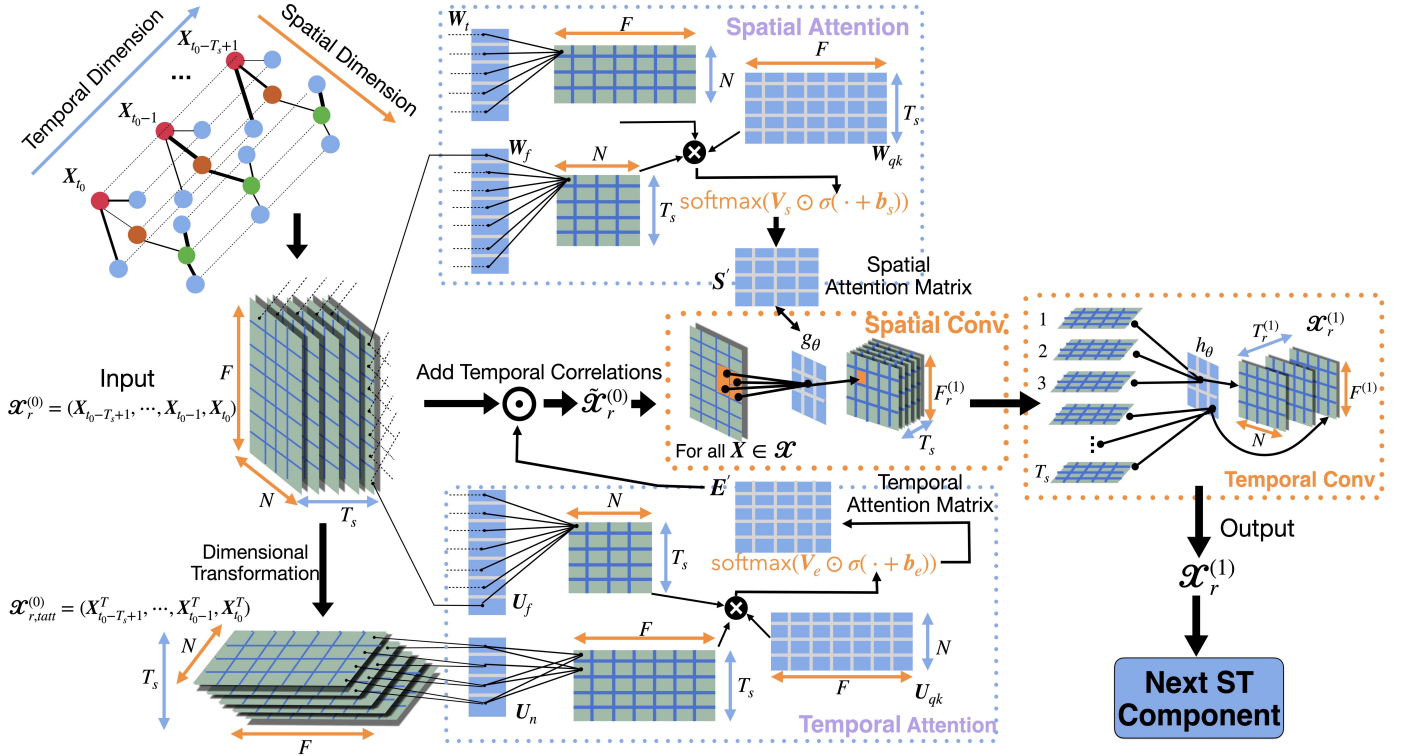


Fig. 5. The process of the recent segment passing through one whole ST component shown in Fig. 4.

3) *Spatial-Temporal Convolution*: The previous ST attention mechanism has introduced both spatial and temporal attention mechanisms, in which their corresponding attention matrices  $S'$  and  $E'$  are adopted for adjusting the original input  $\mathcal{X}$  to ST components. A ST convolution is proposed in this section, consisting of the *spatial graph convolution* and the *temporal standard convolution*, with the aim of not only extracting ST features, but also reducing dimensions of the original input to be applicable for our DRL agent in Section III-B.

**Spatial Graph Convolution:** DN is a graph structure in nature, where features of each node can be considered as signals on the graph [39]. Meanwhile, convolution operation has been generalized from grid-based data to graph-based data in the spectral graph theory [40]. Thus, to better exploit the topological properties of DN, such as degrees of nodes and graph connectivity, a graph convolution operation is proposed here in the spatial view.

In spectral graph theory, the Laplacian matrix is mostly used to represent a graph's structure, in which the properties of a graph can be obtained via analyzing the Laplacian matrix, since it contains two most crucial components in one graph—the adjacency matrix recording mutual influence among nodes; the degree matrix indicating each node's importance [41]. A normalized Laplacian matrix can be formulated as:

$$\mathbf{L} = \mathbf{I} - \mathbf{D}^{-\frac{1}{2}} \mathbf{A} \mathbf{D}^{-\frac{1}{2}} = \mathbf{U} \mathbf{\Lambda} \mathbf{U}^T \in \mathbb{R}^{N \times N}, \quad (48)$$

where  $\mathbf{I}$  is the identity matrix, the degree matrix  $\mathbf{D} \in \mathbb{R}^{N \times N}$  is a diagonal matrix with diagonal element  $\mathbf{D}_{i,i} = \sum_j \mathbf{A}_{i,j}$ ,  $\mathbf{U}$  is the eigenvector matrix of  $\mathbf{L}$ , and  $\mathbf{\Lambda}$  is the diagonal matrix of

eigenvalues of  $\mathbf{L}$ . Both  $\mathbf{U}$  and  $\mathbf{\Lambda}$  are calculated by eigenvalue decomposition.

Graph convolution is defined as a convolution operation implemented by using linear operators which diagonalize in the Fourier domain to replace the classical convolution operator, which can be formulated as [31]:

$$\begin{aligned} \text{ReLU}(g_\theta *_{\mathcal{G}} x) &= \text{ReLU}[g_\theta(\mathbf{L})x] \\ &= \text{ReLU}[\mathbf{U}^T(\mathbf{U}x \odot \mathbf{U}g_\theta)], \end{aligned} \quad (49)$$

where  $x$  represents the input signal,  $g_\theta$  is defined as graph convolution filter,  $*_{\mathcal{G}}$  denotes the graph convolution operation, and rectified linear unit (ReLU) is adopted as activation function of graph convolution operation [38].

Since directly conducting the eigenvalue decomposition is computationally expensive when it comes to a large-scale graph, Chebyshev polynomials are used for efficiently approximating the solution of eigenvalue decomposition [42], which can be formulated as:

$$g_\theta(\mathbf{L})x = \sum_{k=0}^{K-1} \theta_k T_k(\tilde{\mathbf{L}})x, \quad (50)$$

where  $\theta_k$  is the coefficient of Chebyshev polynomials,  $\tilde{\mathbf{L}}$  is expressed as  $\tilde{\mathbf{L}} = \frac{2}{\lambda_{\max}} \mathbf{L} - \mathbf{I}$ , i.e.,  $\lambda_{\max}$  is the maximum eigenvalue of  $\mathbf{L}$ , and  $T_k$  is the  $k$ th-order Chebyshev polynomial. The number of Chebyshev polynomials  $K$  determines the accuracy of approximation, where spatial features of surrounding  $K$  neighbors centered on each node are extracted by the graph convolution kernel  $g_\theta$ . Thus, the bigger  $K$  is, the more accurate information the graph convolution operation gains.

The spatial attention matrix  $\mathbf{S}'$  in Eq. (44) can assign attention weights among nodes to clarify which node pairs are more important in DN graph. Thus, the Chebyshev approximation in Eq. (50) can be rewritten as:

$$g_\theta(\mathbf{L})x = \sum_{k=0}^{K-1} \theta_k \left[ T_k(\tilde{\mathbf{L}}) \odot \mathbf{S}' \right] x. \quad (51)$$

**Temporal Conventional Convolution and Feature Compression:** The conventional convolution operation is conducted on the temporal dimension to capture information in latest power flow reallocation intervals, taking the result of spatial graph convolution operation as input:

$$\mathbf{X}^n = \text{ReLU} \left\{ h_\theta * \left[ \text{ReLU} \left( g_\theta *_{\mathcal{G}} \tilde{\mathbf{X}}^{n-1} \right) \right] \right\}, \quad (52)$$

where  $*$  represents the standard convolution operation,  $\mathbf{X}^n \in \mathbb{R}^{N \times F^n \times T^n}$  is the output of the  $n$ th ST component, and  $h_\theta$  is the standard convolution filter.

To sum up, ST information in DN graph can be fully exploited by MG-ASTGCN. Firstly, spatial attention figures out node pairs' correlation strength while temporal attention extracts self-correlations of each node's features in the temporal view. Then, ST convolution extracts useful features from the DN graph based on the information provided by the preceding attention mechanism. The detailed process of one segment passing through one whole ST component is described in Fig. 5, taking the recent segment as an example.

To apply the results of MG-ASTGCN as the auxiliary graphical information for our DRL agent, the outputs of MG-ASTGCN on different time scales are fused and then passed through a fully-connected neural network layer for compression. Assuming that  $n$  ST components are set for the recent segment input  $\mathbf{X}_r$ , daily segment input  $\mathbf{X}_d$ , and weekly segment input  $\mathbf{X}_w$ , the final output of the proposed MG-ASTGCN  $\mathbf{y}$  is formulated as:

$$\mathbf{y} = \text{ReLU} \left\{ \text{Dense} \left[ \text{concat} \left( \mathbf{X}_r^{n+1}, \mathbf{X}_d^{n+1}, \mathbf{X}_w^{n+1} \right) \right] \right\}, \quad (53)$$

where  $\mathbf{X}_r^{n+1}$ ,  $\mathbf{X}_d^{n+1}$ ,  $\mathbf{X}_w^{n+1}$  represent the output of their corresponding  $n$ th ST component, **concat** represents the concatenating operation for the above three outputs, and **Dense** is defined as a fully-connected layer for feature compression.

### B. Solving MOO-OPF Problem via DRL

To solve the proposed MOO-OPF problem, it is firstly modelled as an MDP, which lays a solid foundation on analyzing specific DRL algorithms. Subsequently, DDPG is adopted to solve the MDP.

1) *MDP Modelling:* Since reallocating power flow can be considered as a consecutive decision-making process, it can be modelled as a dynamic MDP, consisting of four parts:  $(\mathcal{S}, \mathcal{A}, \mathcal{P}, \mathcal{R})$  [16].

**State**  $\mathcal{S}$  represents the state set. Specifically, for the  $i$ th node in DN graph, its state  $s_i^t$  at power flow reallocation interval  $t$  is just the feature vector  $\mathbf{x}_i^t$  proposed in Eq. (37), including its corresponding power, voltage, and surrounding branches' power.

**Action**  $\mathcal{A}$  is defined as the action set. For each power generator, only their active power  $P_i^t$  and voltage  $\mathbb{V}_i^t$  can

---

### Algorithm 1 DDPG Algorithm

---

Randomly initialize action policy  $\pi_\theta(\mathbf{s})$  and critic network  $Q^\pi(\mathbf{s}, \mathbf{a})$  with weights  $\theta^Q$  and  $\theta^\pi$

Initialize target networks  $\pi_{\theta'}$  and  $Q^{\pi'}$  with weights  $\theta^{Q'} \leftarrow \theta^Q$ ,  $\theta^{\pi'} \leftarrow \theta^\pi$

Initialize the replay buffer  $\mathcal{B}$  with sufficient capacity

**for**  $n = 1, 2, \dots, N_\tau$  **do**

Initialize a random process  $\mathcal{N}$  for action exploration

Reset the original state  $\mathbf{s}^1$

Reset the cumulative reward  $R_c \leftarrow 0$

**for**  $t = 1, 2, \dots, T_n$  **do**

Select action  $\mathbf{a}^t = \pi_\theta(\mathbf{s}^t) + \mathcal{N}$  based on current action policy  $\pi^\theta$  and exploration noise  $\mathcal{N}$

Interact with the environment using action  $\mathbf{a}^t$  and get reward  $r^t$  and the next state  $\mathbf{s}^{t+1}$

**if** *PowerFlowNotConverged* **then**

**Break**

**end if**

Update the cumulative reward  $r_c \leftarrow r_c + r^t$

**if**  $r_c > r_{es}$  **then**

**Break**

**end if**

Store a transition  $\{\mathbf{s}^t, \mathbf{a}^t, r^t, \mathbf{s}^{t+1}\}$  in  $\mathcal{B}$

Randomly sample a batch of  $N$  transitions from  $\mathcal{B}$ .

Calculate  $q^t$  using the target networks,  $q^t \leftarrow r^t + \gamma Q^{\pi'}[\mathbf{s}^{t+1}, \pi_{\theta'}(\mathbf{s}^{t+1})]$

Update the critic network  $Q^\pi$  by using gradient descent to minimizing the RMSE function  $L(Q^\pi) = \frac{1}{N} \sum_i [Q^\pi(\mathbf{s}^t, \mathbf{a}^t) - q^t]^2$ :

$\theta^Q \leftarrow \theta^Q - \eta_Q \nabla_Q L(Q^\pi)$

Update the action policy  $\pi_\theta$  by policy gradient:

$\theta^\pi \leftarrow \theta^\pi - \eta_{\pi_\theta} \nabla_{\theta} R_\theta$

Update target networks using the soft update method with its corresponding parameter  $\rho$ :

$\theta^{Q'} \leftarrow \rho \theta^Q + (1 - \rho) \theta^{Q'}$

$\theta^{\pi'} \leftarrow \rho \theta^\pi + (1 - \rho) \theta^{\pi'}$

**end for**

**end for**

---

be manipulated. Thus, the action space of the  $i$ th node can be expressed as:  $a_i^t = \{P_i^t, \mathbb{V}_i^t\}$ . The reallocation of each generator's active power and voltage has a direct impact on not only its local features, such as branch power flow  $\mathbb{S}_{i,j}$ , but also other nodes' power flow reallocation.

**Probability**  $\mathcal{P}$  is the probability of a transition to the next state  $s_i^{t+1}$  from the current state  $s_i^t$  after choosing the action  $a_i^t$ , which can be formulated as  $p(s_i^{t+1} | s_i^t, a_i^t)$ . Note that calculating the probability is inapplicable since  $s_i^{t+1}$  is deterministic by the environment once  $s_i^t$  and  $a_i^t$  are determined. Instead, in RL, an action strategy is learned to let the model how to deal with different states, denoted by  $\pi : \mathcal{S} \rightarrow \mathcal{P}(\mathcal{A})$ , which maps states to a probability distribution over actions. More details regarding learning an action strategy are introduced in Section III-B2.

**Reward**  $\mathcal{R}$  represents the reward set, where reward  $r_i^t$  is obtained from the environment after taking action  $a_i^t$  at



current state  $s_i^t$ . The goal of RL is to maximize the reward using our trained agent action strategy  $\pi$ , which is equal to minimizing the proposed MOO-OPF problem in Section II-B. Thus, designing an appropriate reward function  $R$  based on the objective functions from Eq. (12) to (13), taking into account all optimization constraints, plays a significant role in training a RL agent. In this paper, a reward function  $R(\cdot)$ , consisting of 8 sub-reward functions from  $r_1(\cdot)$  to  $r_8(\cdot)$ , is proposed to reduce generation cost, alleviate voltage fluctuation when connected to RERs, and meet the operational constraints in DN, which can be formulated as:

$$R = \sum_{i=1}^8 w_i r_i, \quad r_i \leftarrow \tilde{r}_i, \quad i = 5, 6, 7, \quad (54)$$

$$r_1 = - \sum_{i=1}^{N_t} C_{t,i}(\cdot) - \sum_{j=1}^{N_w} C_{w,j}^{\text{d,rp}}(\cdot) - \sum_{k=1}^{N_s} C_{s,k}^{\text{d,rp}}(\cdot), \quad (55)$$

$$r_2 = -\frac{1}{r^1} \cdot \frac{P^1}{\sum_{i=1}^{N_g} P_i}, \quad (56)$$

$$r_3 = 1 - \frac{1}{N_b} \sum_{i=1}^{N_b} \min\left(\frac{I_i}{T_i + \varepsilon}, 1\right), \quad (57)$$

$$r_4 = -F^V, \quad (58)$$

$$r_5 = \frac{1}{N_g} \begin{cases} \sum_{i=1}^{N_g} \left(1 - \frac{P_i}{\bar{P}_i}\right), & \forall P_i > \bar{P}_i, \\ \sum_{i=1}^{N_g} \left(1 - \frac{P_i}{\underline{P}_i}\right), & \forall P_i < \underline{P}_i, \end{cases} \quad (59)$$

$$\tilde{r}_5 = \exp(r_4) - 1, \quad (60)$$

$$r_6 = \frac{1}{N_g} \begin{cases} \sum_{i=1}^{N_g} \left(1 - \frac{Q_i}{\bar{Q}_i}\right), & \forall Q_i > \bar{Q}_i, \\ \sum_{i=1}^{N_g} \left(1 - \frac{Q_i}{\underline{Q}_i}\right), & \forall Q_i < \underline{Q}_i, \end{cases} \quad (61)$$

$$\tilde{r}_6 = \exp(r_5) - 1, \quad (62)$$

$$r_7 = \frac{1}{N} \begin{cases} \sum_{i=1}^N \left(1 - \frac{|\mathbb{V}_i|}{\bar{V}_i}\right), & \forall |\mathbb{V}_i| > \bar{V}_i, \\ \sum_{i=1}^N \left(1 - \frac{|\mathbb{V}_i|}{\underline{V}_i}\right), & \forall |\mathbb{V}_i| < \underline{V}_i, \end{cases} \quad (63)$$

$$\tilde{r}_7 = \exp(r_6) - 1, \quad (64)$$

$$r_8 = \frac{\sum_{i=1}^{N_w+N_s} P_i}{\sum_{i=1}^{N_w+N_s} \bar{P}_i}, \quad (65)$$

where  $N^g$  is the total number of generators, which can be formulated as:

$$N^g = N^t + N^w + N^s, \quad (66)$$

and  $C_{w,j}^{\text{d,rp}}$  and  $C_{s,k}^{\text{d,rp}}$  represent the summation of direct cost, reserve cost, and penalty cost in wind and solar PV power, respectively, which can be expressed as:

$$C_{w,j}^{\text{d,rp}} = C_{w,j}^{\text{d}} + C_{w,j}^{\text{r}} + C_{w,j}^{\text{p}}, \quad (67)$$

$$C_{s,k}^{\text{d,rp}} = C_{s,k}^{\text{d}} + C_{s,k}^{\text{r}} + C_{s,k}^{\text{p}}. \quad (68)$$

- $r_1(\cdot)$  is defined as a negative reward function, representing the direct cost of power generation.
- $r_2(\cdot)$  and  $r_3(\cdot)$  are both designed to describe the transmission power loss.  $r_2(\cdot)$  represents the actual line loss rate compared to the standard line loss rate  $r^1$ . The power on each branch is usually assessed using its corresponding current  $I_i$  and thermal current limit  $T_i$  as proposed in

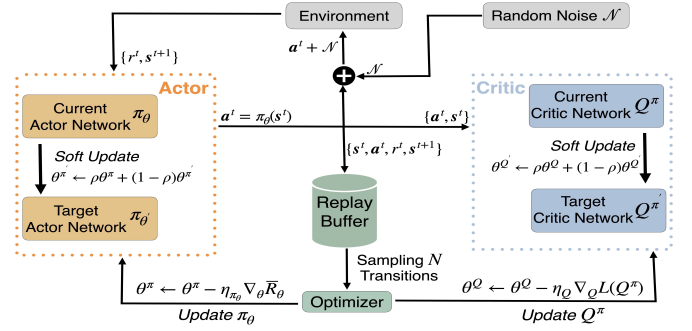


Fig. 6. The workflow of DDPG for solving the MOO-OPF problem.

$r_3(\cdot)$  [27], where a very small constant  $\varepsilon$  is adopted to ensure that denominator is not zero.

- $r_4(\cdot)$  is proposed to control the voltage fluctuation when connected to RERs.
- $r_5(\cdot)$  to  $r_7(\cdot)$  are developed based on the MOO-OPF problem's constraints presented from Eq. (17) to (27).
- Since the adoption of RERs to conventional power systems aims to reduce carbon emission,  $r_8(\cdot)$  is designed to incentivize the DN to accommodate as many RERs as possible.
- $w_i, i = 1, \dots, 8$  is the weight coefficient of the reward function. The analysis of setting different  $w_i$  values is presented in Section IV-B.
- All features mentioned in reward functions have been normalized before calculation.

The objective of RL is to maximize the expected reward  $\bar{R}_\theta$  based on our learned agent's action policy  $a = \pi_\theta(s)$  [16], expressed as:

$$\begin{aligned} \bar{R}_\theta &= \mathbb{E}_{a^t \sim \pi, r^t, s^{t+1} \sim \text{Env}} [R(\tau)] \\ &= \sum_{\tau} R(\tau) P(\tau | \theta), \end{aligned} \quad (69)$$

where  $\theta$  is presented as parameters of the policy  $\pi$ , and  $\tau$  can be considered as one trajectory of adjusting power flow till its convergence, i.e., reaching the optimal power flow, recording all the 4-tuple transitions  $\{s^t, a^t, r^t, s^{t+1}\}$  from the beginning of  $\tau$  to its end.

2) *Solving MDP by DDPG*: DDPG is one representative of the actor-critic RL algorithm family, which achieves the state-of-the-art performance in optimizing the proposed MDP objective in Eq. (69) with its continuous action space  $a_i^t = \{P_i^t, \mathbb{V}_i^t\}$  [43]. The biggest difference between DDPG and other RL algorithms is that the agent action policy  $a = \pi_\theta(s)$  deterministically outputs the values of action vector instead of the probability distribution of action, which dramatically decreases the computation cost and make it much easier to implement. The workflow of applying DDPG to solve the MOO-OPF problem is presented in Fig. 6.

The policy gradient method is applied in DDPG to update our agent action policy  $\pi_\theta$  so as to maximize the expected reward by gradient descent, which can be formulated as:

$$\theta \leftarrow \theta - \eta \nabla \bar{R}_\theta, \quad (70)$$

where  $\eta$  is the learning rate, and the gradient of the expected reward can be rewritten as [16]:

$$\nabla \bar{R}_\theta = \frac{1}{N_\tau} \sum_{n=1}^{N_\tau} \sum_{t=1}^{T_n} A^\theta(\mathbf{s}_n^t, \mathbf{a}_n^t) \nabla \log p(\mathbf{a}_n^t | \mathbf{s}_n^t, \theta), \quad (71)$$

where  $N_\tau$  is the total number of trajectories our agent has sampled,  $T_n$  is the length of the  $n$ th trajectory,  $\mathbf{s}_n^t$  and  $\mathbf{a}_n^t$  are the state vector and action vector including all nodes' states and actions in DN, respectively, denoted as  $\mathbf{s}_n^t = \text{flatten}\{\text{concat}[(\mathbf{s}_1^t, \mathbf{s}_2^t, \dots, \mathbf{s}_N^t, \mathbf{y}^t)]\}$  and  $\mathbf{a}_n^t = \text{flatten}\{\text{concat}[(\mathbf{a}_1^t, \mathbf{a}_2^t, \dots, \mathbf{a}_N^t)]\}$ . The **flatten** operation is to transform the result of concatenation into one-dimension vector. Note that  $\mathbf{s}_n^t$  also contains the output of MG-ASTGCN  $\mathbf{y}^t$  in Eq. (53) as auxiliary information. The above advantage function  $A^\theta(\mathbf{s}_n^t, \mathbf{a}_n^t)$  can be expressed as:

$$A^\theta(\mathbf{s}_n^t, \mathbf{a}_n^t) = G_n^t - b, \quad (72)$$

$$G_n^t = \sum_{t'=t}^{T_n} \gamma^{t'-t} r_{t'}^n, \quad b = \mathbb{E}_{\mathbf{s} \sim \text{Env}} [R(\mathbf{s})], \quad (73)$$

where  $G_n^t$  is the summation of future rewards with a discounting factor  $\gamma \in [0, 1]$ , and  $b$  is the baseline of reward considering all possible actions.

The advantage function is a criterion to assess how good the chosen action  $\mathbf{a}_n^t$  is under current state  $\mathbf{s}_n^t$  compared to baseline. Due to the uncertainties of the environment, it is obvious that both  $G_n^t$  and  $b$  are random variables. Thus, it is inevitable to estimate the proposed advantage function, which has been achieved by a critic network,  $Q^\pi(\mathbf{s}^t, \mathbf{a}^t)$  in DDPG, which can be formulated as:

$$Q^\pi(\mathbf{s}^t, \mathbf{a}^t) = \mathbb{E}_{r^t, \mathbf{s}^{t+1} \sim \text{Env}} \{r^t + \gamma Q^\pi[\mathbf{s}^{t+1}, \pi_\theta(\mathbf{s}^{t+1})]\}. \quad (74)$$

The advantage function in Eq. (72) is estimated using the critic network, which can be formulated as:

$$A^\theta(\mathbf{s}_n^t, \mathbf{a}_n^t) = Q^\pi(\mathbf{s}_n^t, \mathbf{a}_n^t) - \sum_{\mathbf{a}_n^t} Q^\pi(\mathbf{s}_n^t, \mathbf{a}_n^t). \quad (75)$$

Since the expectation calculation in Eq. (74) depends on the environment rather the action policy  $\pi$ , it is applicable to learn the  $Q^\pi$  in an off-policy way of using transitions generated from a different agent action policy  $\pi_{\theta'}$ . The critic network can be updated by minimizing the root mean square error (RMSE):

$$L(Q^\pi) = \mathbb{E}_{\mathbf{s}^t, r^t \sim \text{Env}, \mathbf{a}^t \sim \pi_{\theta'}} \left\{ [Q^\pi(\mathbf{s}^t, \mathbf{a}^t) - q^t]^2 \right\}, \quad (76)$$

where

$$q^t = r^t + \gamma Q^\pi[\mathbf{s}^{t+1}, \pi_\theta(\mathbf{s}^{t+1})]. \quad (77)$$

**Termination Criterion for Training DDPG:** Searching for the OPF is based on the fact that power flow has reached convergence. Therefore, at each timestep  $t$  in a training episode  $n$ , the training episode should be terminated if the power flow is not converged. The convergence condition for DN is formulated as:

$$\|\mathbf{v}_i^t - \mathbf{v}_i^{t-1}\| \leq \epsilon, \quad \forall i \in \mathcal{V}, \quad (78)$$

where  $\epsilon$  is the mismatch tolerance to measure the distance between  $\mathbf{v}_i^t$  and  $\mathbf{v}_i^{t-1}$ .  $\mathbf{v}_i^t$  and  $\mathbf{v}_i^{t-1}$  represent characteristics

TABLE I  
SYSTEM CHARACTERISTICS IN IEEE 33-BUS, 69-BUS, AND 118-BUS RDSs.

RDSs Characteristics	33-Bus	69-Bus	118-Bus
Total Buses ( $N_t$ )	33	69	118
Thermoelectric Generators ( $N_t$ )	2	3	4
Wind Turbines ( $N_w$ )	5	10	15
Solar PV Generators ( $N_s$ )	5	10	15
Baseline Voltage (kV)	12.66	12.66	11
Baseline Apparent Power (MVA)	100	100	100
Total Load Active Power (MW)	3.715	3.800	22.710
Total Load Reactive Power (MVAR)	2.300	2.690	17.041

of the  $i$ th node in the DN graph  $\mathcal{G}$  at power flow reallocation interval  $t$  and  $t-1$ , respectively, which can be formulated as:

$$\mathbf{v}_i^t = (P_i^t, Q_i^t, \mathbb{V}_i^t)^T, \quad (79)$$

$$\mathbf{v}_i^{t-1} = (P_i^{t-1}, Q_i^{t-1}, \mathbb{V}_i^{t-1})^T, \quad (80)$$

Additionally, early stopping is applied when implementing the DDPG, which calculates the cumulative reward  $r_c$  for every training episode  $n$ .  $r_c$  can be formulated as:

$$r_c = \sum_{t=1}^{t'} r^t, \quad (81)$$

where  $t'$  represents the current training timestep.

Once the  $r_c$  exceeds the early stopping's threshold  $r_{es}$ , its corresponding training episode will be terminated. The adoption of early stopping aims to not only prevent the DRL agent from learning unsatisfactory policy to reallocate the power flow, but also accelerate its convergence speed.

In summary, DDPG follows the policy-gradient way to solve the objective of the proposed MDP, where a critic network is introduced to assess our learned agent action policy. The corresponding algorithm process is illustrated in Algorithm 1.

## IV. EXPERIMENTS

### A. Experimental Settings

1) *Application Scenario:* The proposed DRL-based approach is tested on the modified IEEE 33-bus, 69-bus, and 118-bus radial distribution systems (RDSs), whose structures are illustrated in Fig. 7. The three RDSs characteristics include the number of generators, baseline voltage, baseline apparent power, load active power, and load reactive power, as presented in Table I.

2) *Parameter Initialization:* The initialized parameters regarding voltage fluctuation control, uncertainty models of wind and solar PV power [44], [45], MG-ASTGCN, and DDPG are presented in Table II. Note that parameters of each wind turbine and solar PV generator are slightly different, where parameters in Table II, for simplicity, only represent one wind turbine and solar PV generator, respectively.



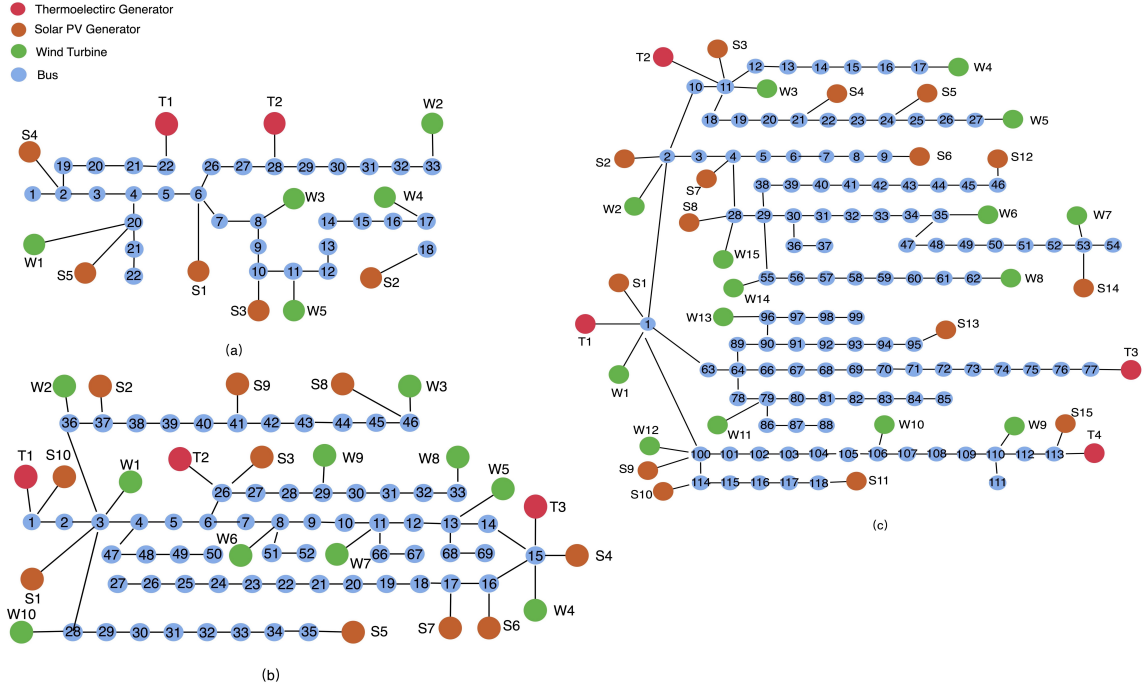


Fig. 7. The structures of modified IEEE 33-bus, 69-bus, and 118-bus RDSs, shown in (a), (b), and (c), respectively.

TABLE II  
THE PARAMETER INITIALIZATION FOR UNCERTAINTY MODELS OF WIND  
AND SOLAR PV POWER, VOLTAGE FLUCTUATION CONTROL,  
MG-ASTGCN, AND DDPG.

	Parameter	Value
<b>Wind Turbine</b>	$p_w^t$ (MW)	75
	$c$	9
	$k$	2
	$\mathbb{E}(v)$ (m/s)	7.976
<b>Solar PV Generator</b>	$p_s^t$ (MW)	50
	$\mu$	6
	$\sigma$	0.6
	$\mathbb{E}(G)$ (W/m)	483
<b>Voltage Control</b>	$T_{ld}$	10
	$T_r$	50
	$T_d$	10
<b>MG-ASTGCN</b>	$T_w$	3
	ST Components	3
	<b>DDPG</b>	$N_\tau$
$T_n$		150
$r_{es}$		-100, -200, -300 (for 33, 69, and 118 bus RDSs, respectively)
$w_1 \sim w_8$		1
$\epsilon$		0.0001

3) *Algorithm Performance Metric*: The reward functions presented from Eq. (54) to (65) can also be adopted to measure the performance of other algorithms, since these reward functions are designed to satisfy DN's operating constraints, evaluate voltage fluctuation, and accommodate as many RERs as possible. Here, we introduce a criterion to assess algorithms for solving the MOO-OPF problem, which can be calculated as:

$$\text{SCORE} = \frac{1}{N_{\text{eva}}} \sum_{n=1}^{N_{\text{eva}}} \sum_{t=1}^{T_{\text{end}}} R_n^t, \quad (82)$$

where  $N_{\text{eva}}$  is the number of episodes for evaluation,  $T_{\text{end}}$  is the length of one episode, and  $R_n^t$  has been defined in Eq. (54). Both  $N_{\text{eva}}$  and  $T_{\text{end}}$  are initialized to 100. The detailed process of evaluating one algorithm is presented in Algorithm 2.

## B. Experimental Results

1) *Comparison with Other DRL Algorithms*: In the proposed DRL-based approach, DDPG is adopted for solving the MOO-OPF problem. To evaluate the effectiveness of DDPG, we also train several other DRL algorithms with the same hyperparameters as DDPG, such as proximal policy optimization (PPO) [46], actor-critic with experience replay (ACER) [47], soft actor-critic (SAC) [48], advantage actor-critic (A2C) [49]. A workstation with 5 Nvidia TITAN RTX graphics processing units and Intel(R) Xeon(R) Silver 4210 central processing units is used for the DRL training. The training rewards in these above four DRL algorithms, together with DDPG, are illustrated in Fig. 8. The evaluation results of DRL algorithms are presented in Table III.

DRL algorithms can be categorized into on-policy and off-policy algorithms, where on-policy algorithms such as PPO and A2C have faster sampling efficiency while off-policy algorithms such as A2C, ACER, SAC, and DDPG make full use of the historical data [16]. Under our scenario, training the on-policy algorithms such as PPO and A2C seems to be more time-consuming according to Table III, where their corresponding training time per episode is much smaller than the off-policy algorithms. However, due to the complexity of both DN and MDP state space, it is challenging for them to select better action for reallocating power flow totally based on their current sampled data, which leads to their low

TABLE III  
THE AVERAGE TRAINING TIME AND EVALUATION RESULTS OF DRL ALGORITHMS.

DRL Algorithm	Average Training Time in 33-bus RDS	SCORE in 33-bus RDS	Average Training Time in 69-bus RDS	SCORE in 69-bus RDS	Average Training Time in 118-bus RDS	SCORE in 118-bus RDS
A2C	30.81s /episode	2783.74	78.02s /episode	5280.29	104.64s /episode	7531.95
ACER	39.23s /episode	3454.69	95.26s /episode	6714.91	135.77s /episode	8814.45
PPO	<b>31.64s</b> /episode	3557.12	<b>75.39s</b> /episode	6691.93	<b>102.84s</b> /episode	10997.55
SAC	37.83s /episode	3940.75	86.33s /episode	7662.38	125.98s /episode	12133.61
<b>DDPG (Ours)</b>	37.45s /episode	<b>4014.59</b>	84.90s /episode	<b>7756.64</b>	125.74s /episode	<b>14384.11</b>

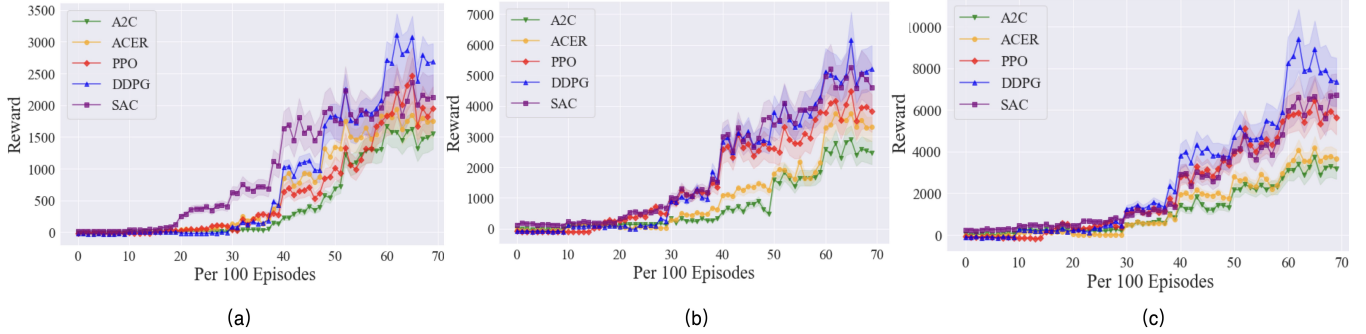


Fig. 8. The reward curves of DRL algorithms during the training process in IEEE 33-bus, 69-bus, and 118-bus RDSs shown in (a), (b), and (c), respectively.

SCOREs. Meanwhile, sampling real-time power flow can be expensive in the actual DN which makes implementing on-policy algorithms more inapplicable. Although it needs more time to train a well-performed off-policy algorithm, which is about 40s per episode in IEEE 33-bus RDS, it is still preferred in practice, since the adoption of historical data in their training processes results in better exploration and exploitation abilities in such complicated and dynamic environment.

Additionally, from Table III and Fig. 8, it can be observed that DDPG shows its best performance in all three RDSs, i.e., lower training time and higher SCORE than other two off-policy algorithms. Notably, the disparity between DDPG and other two algorithms gradually increases from the 33-bus to the 118-bus RDS. Therefore, we can draw the conclusion that DDPG has a better capability of solving the MOO-OPF problem, especially in a large-scale DN.

2) *Comparison with Benchmark Algorithms:* Two representative heuristic algorithms—harris hawk optimization (HHO) [50] and grey wolf optimization (GWO) [9], are adopted to solve the MOO-OPF problem as well. The testing results of these two heuristic algorithms, together with the proposed DRL-based approach, are presented in Table VII. It shows that the proposed DRL-based approach totally outperforms HHO, and GWO algorithms, which consumes much less time to reallocate power flow at each timestep while achieving outstanding performance. Indeed, two properties of these algorithms mainly lead to this performance gap, which can also be observed from evaluation results illustrated Fig. 9:

- Heuristic algorithms do not need training, which results in longer computation time at each timestep. Meanwhile, since they tend to get stuck in local optima, their selected actions at each timestep are not the optimal ones, which corresponds to smaller rewards from the environment in

**Algorithm 2** Calculating SCORE for algorithm evaluation

```

Initialize SCORE ← 0
for n = 1, 2, ..., Neva do
  Reset original state s1
  Initialize cumulative reward Rn ← 0
  for t = 1, 2, ..., Tend do
    Determine current action at based on the input algorithm
    Get reward rt and st+1 by interacting with DN
    Update cumulative reward Rn ← Rn + rt
    if PowerFlowNotConverged then
      Break
    end if
  end for
  Update SCORE:
  SCORE ← SCORE + Rn
end for
Calculate average SCORE:
SCORE ← 1/Neva SCORE.

```

Fig. 9.

- The tremendous historical data adopted in the DRL-based approach’s training results in its more effective and efficient searching in the environmental action space. Therefore, it reacts much faster at the beginning of the evaluation and gradually gets a higher SCORE, especially in the modified IEEE 118-bus RDS.

3) *Effectiveness of ST Attention Mechanism:* To test the effectiveness of ST attention mechanism and its impact on the sequential DRL-based approach, i.e., DDPG, the ST attention mechanism is substituted with several similar techniques, such as cosine similarity (CS), and jaccard similarity (JS) [51],

TABLE IV  
THE AVERAGE TESTING TIME AND EVALUATION RESULTS OF THE PROPOSED DRL-BASED APPROACH, HHO, AND GWO ALGORITHMS.

Model	Average Testing Time in 33-bus RDS	SCORE in 33-bus RDS	Average Testing Time in 69-bus RDS	SCORE in 69-bus RDS	Average Testing Time in 118-bus RDS	SCORE in 118-bus RDS
HHO	2.35s /timestep	3530.66	6.12s /timestep	6104.81	12.69s /timestep	8231.95
GWO	3.44s /timestep	3014.44	8.12s /timestep	5821.99	15.79s /timestep	7481.24
<b>DRL (Ours)</b>	<b>0.89s /timestep</b>	<b>4014.59</b>	<b>1.26s /timestep</b>	<b>7756.64</b>	<b>1.57s /timestep</b>	<b>14384.11</b>

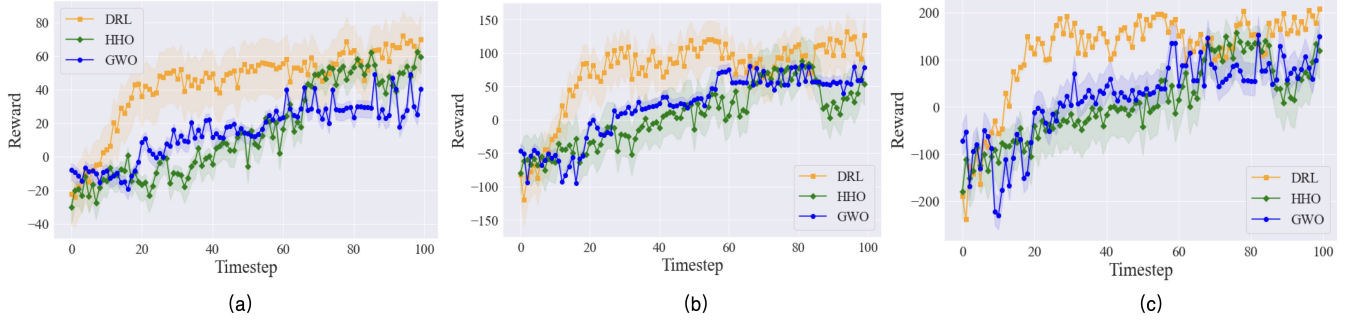


Fig. 9. Evaluation SCOREs of HHO, GWO, and DRL algorithms in IEEE 33, 68, and 118-bus RDSs shown in (a), (b), and (c), respectively.

TABLE V  
THE EVALUATION RESULTS REGARDING DIFFERENT SUBSTITUTIONS OF ST ATTENTION MECHANISM.

Models	SCORE in 33-bus RDS	SCORE in 69-bus RDS	SCORE in 118-bus RDS
DRL	1843.72	3913.58	5031.49
CS+DRL	2341.95	4285.56	6357.11
JS+DRL	2099.62	3985.66	5579.38
<b>ST Attention+DRL (Ours)</b>	<b>4014.59</b>	<b>7756.64</b>	<b>14384.11</b>

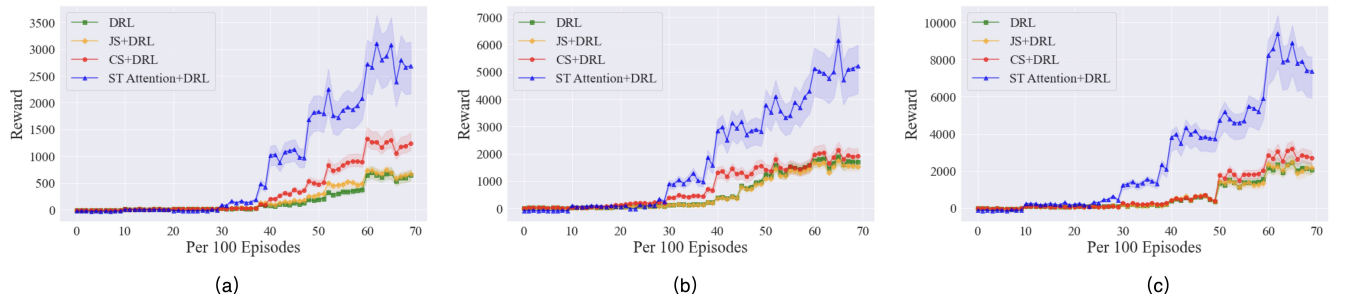


Fig. 10. Training reward curves with different graph correlation extraction methods, i.e., pure DRL, CS+DRL, JS+DRL, and ST Attention+DRL.

which can also calculate the correlation among nodes in a DN graph, and are formulated as:

$$s_{i,j}^{cs} = \frac{\mathbf{a}_i \cdot \mathbf{a}_j}{\|\mathbf{a}_i\| \cdot \|\mathbf{a}_j\|}, \quad (83)$$

$$s_{i,j}^{js} = \frac{\sum_k \min\{a_i^k, a_j^k\}}{\sum_k \max\{a_i^k, a_j^k\}}, \quad (84)$$

where  $s_{i,j}^{cs}$  and  $s_{i,j}^{js}$  are the correlation strengths obtained by CS and JS, respectively, and  $\mathbf{a}_i$  and  $\mathbf{a}_j$  are the  $i$  and  $j$ th rows in the adjacency matrix  $\mathbf{A}$ , respectively. Their corresponding training and evaluation results are shown in Fig. 10 and Table V, respectively. Note that the ST convolution is kept while we only substitute its previous ST attention.

We can draw several conclusions regarding the effect of ST attention as follows.

- The adoption of ST Attention can dramatically increase its sequential DRL algorithm’s convergence speed, where more effective searching with higher reward in the potential large action space is conducted.
- It is challenging for a pure DRL-based approach that has no graph correlation extraction to tackle the complex MOO-OPF problem, since both the action space and state space in the given DN is super large.
- The substituted methods for graph correlation extraction are less effective than ST attention, since both CS and JS only focus on the degree correlation among different nodes, which ignores each node’s inner features, i.e.,

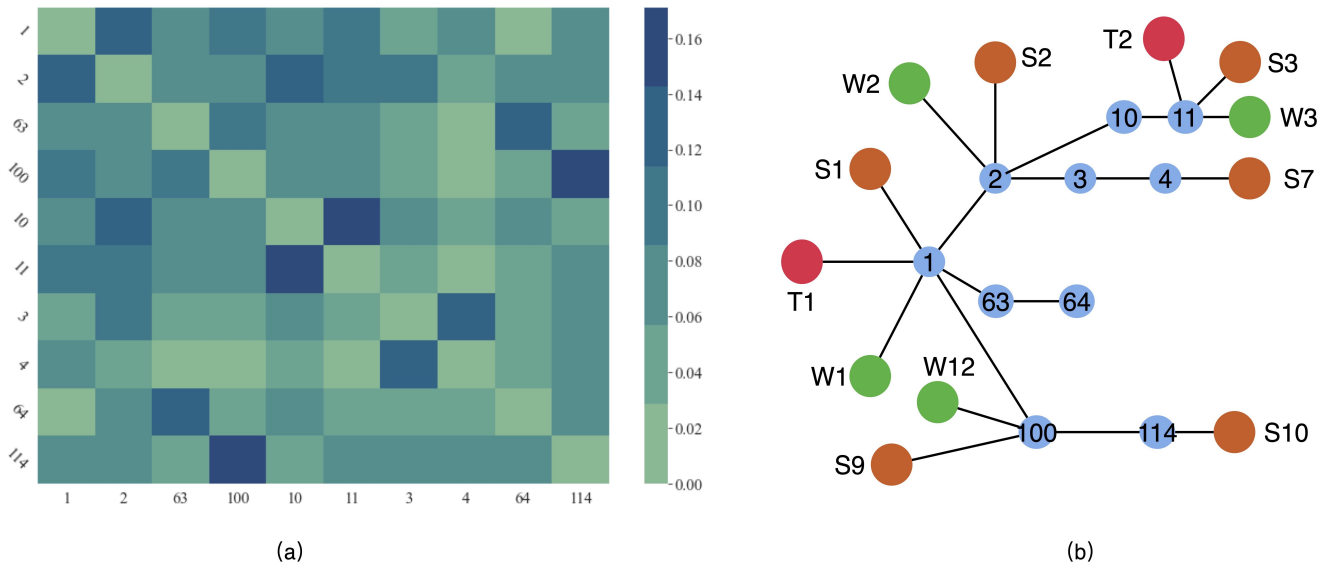


Fig. 11. The partial spatial attention matrix in IEEE 118-bus RDS. Since the total spatial attention matrix is large, for simplicity, Buses 1, 2, 63, 100, 10, 11, 3, 4, 64, 114 are selected for display. The sub-graph including these buses are shown in (b).

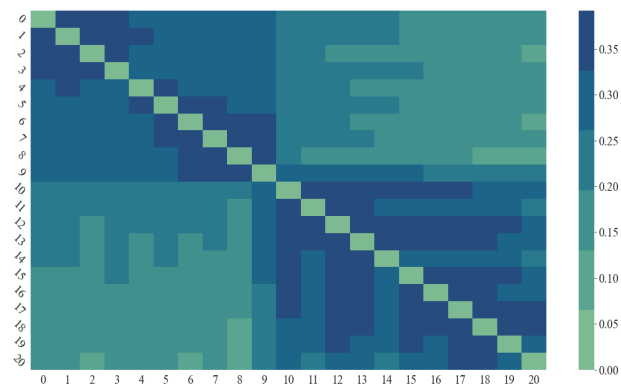


Fig. 12. The partial recent temporal matrix of Bus 1 in IEEE 118-bus RDS. The dimension of recent temporal attention matrix is  $50 \times 50$ . For simplicity, only the latest 20 reallocation intervals are included for display.

voltage, power, and etc. On the contrary, ST attention calculates correlation strengths among nodes based on their feature vectors which are the foundation for power flow reallocation. Meanwhile, ST attention also considers the temporal correlation of each node’s characteristics, which is not included by CS and JS.

Additionally, we find two interesting conclusions about DN from the temporal and spatial attention matrices, which are illustrated in Fig. 11 and 12, respectively.

- In Fig. 11, the spatial attention mechanism tends to focus on node pairs with more generator access, which means larger weights are assigned to their correlation strengths. For instance, although Bus 2 and 114 are not adjacency, they can be connected by Bus 1 and 100, where 2 and 3 power generators are connected, respectively. Therefore, it is reasonable that the correlation between Bus 2 and 114 is more significant than other nonadjacent node pairs.
- In Fig. 12, in the recent temporal attention, the correlation

TABLE VI  
THE EVALUATION RESULTS WITH DIFFERENT VOLTAGE FLUCTUATION WEIGHT.

$w_4$	SCORE in 33-bus RDS	SCORE in 69-bus RDS	SCORE in 118-bus RDS
1	<b>4014.59</b>	<b>7756.64</b>	<b>14384.11</b>
2	3979.14	7544.81	13958.24
3	3967.51	7394.53	13572.31
4	3843.72	7252.66	12891.59
5	3687.13	7036.29	12186.67

strengths between current and previous node features drop sharply when it comes to the 10th previous node feature vector, where we can conclude that the latest 10 feature vectors of one node contain more significant temporal correlation information.

4) *Voltage Fluctuation Control*: The weights assigned for each reward function described from Eq. (54) to (65) represents their corresponding importance. We conduct several evaluation experiments with different *voltage fluctuation weight*, i.e., weight  $w_4$  in reward function  $r_4(\cdot)$  defined in Eq. (58), to test the proposed DRL-based approach’s capability in dealing with volatge fluctuation. Voltage fluctuation of Bus 15 in IEEE 69-bus RDS is illustrated in 13 while detailed evaluation results are presented in Table VI.

Interestingly, although the voltage fluctuation is well-controlled with the increase of  $w_4$ , the DRL agent seems to get stuck in local optimums, i.e., the SCOREs with  $w_4$  from 2 to 4 are lower than its initialized value. Moreover, the DRL-based approach’s performance with larger  $w_4$  degenerates when it comes to large-scale DNs. We can conclude that the proposed DRL-based approach will find the sub-optimal operation point of DN if voltage fluctuation control is overemphasized.

5) *Stability Test of DRL*: The average response time is defined to assess the stability of DN using different MOO-OPF



TABLE VII  
THE AVERAGE RESPONSE TIME OF THE PROPOSED DRL-BASED APPROACH, HHO, AND GWO ALGORITHMS.

Number of Node Removal	Model	Average Response Time in 33-bus RDS	Average Response Time in 69-bus RDS	Average Response Time in 118-bus RDS
1	HHO	9.41	15.17	24.27
	GWO	12.85	20.87	31.51
	<b>DRL (Ours)</b>	<b>5.93</b>	<b>11.96</b>	<b>18.58</b>
Number of Node Removal	Model	Response Time in 33-bus RDS	Response Time in 69-bus RDS	Response Time in 118-bus RDS
2	HHO	13.15	20.72	29.38
	GWO	15.75	25.03	37.14
	<b>DRL (Ours)</b>	<b>9.86</b>	<b>15.59</b>	<b>22.88</b>
Number of Node Removal	Model	Response Time in 33-bus RDS	Response Time in 69-bus RDS	Response Time in 118-bus RDS
3	HHO	15.89	27.98	42.51
	GWO	16.17	29.53	41.47
	<b>DRL (Ours)</b>	<b>12.57</b>	<b>21.68</b>	<b>32.82</b>

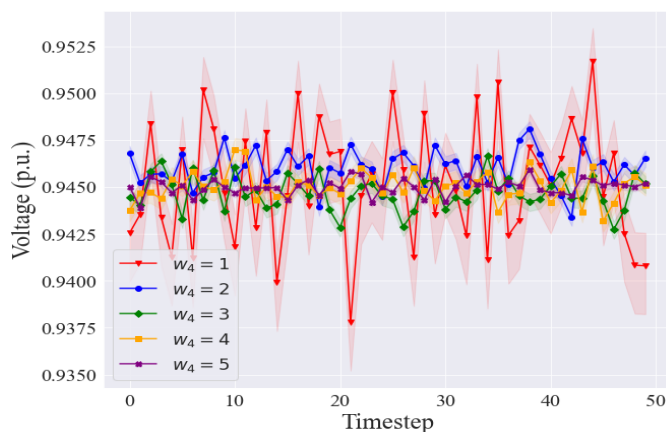


Fig. 13. Voltage fluctuation of Bus 15 in IEEE 69-bus RDS with different voltage fluctuation weight.

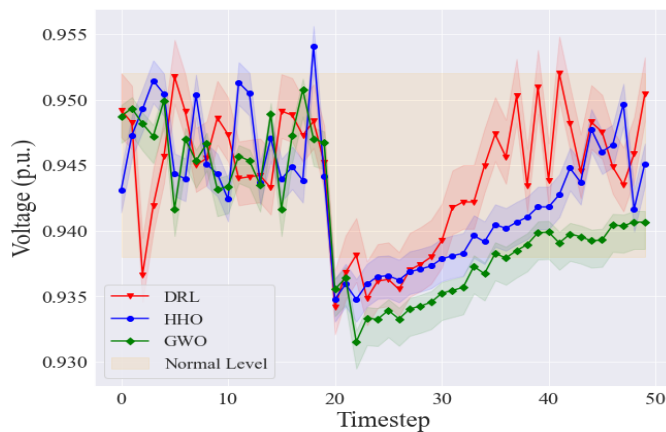


Fig. 14. Response time of HHO, GWO, and the proposed DRL-based approach when one generator is removed from Bus 15 in IEEE-69 bus RDS. Assume that the removal occurs at the 20th timestep.

solutions when facing node faults, which describes how many timesteps the DN needs to recover every node’s voltage to its normal level. We conduct several experiments with a different number of generator removals, where one specific case is illustrated in Fig. 14. Obviously, the proposed DRL-based approach has the shortest response time, especially for the IEEE-118 bus RDS, which means the adoption of the proposed DRL-based approach can significantly improve DN’s stability. The detailed statistics about this experiment are presented in VII.

## V. CONCLUSIONS AND FUTURE WORKS

In this paper, we have proposed a DRL-based approach, which is accompanied by multi-grained ST graph information, to not only alleviate uncertainties brought in by RERs, but also improve DN’s stability, which can achieve more dynamic, rapid, and effective optimal operation adjustment in DNs. First, we derive the MOO-OPF formulation considering the high renewable penetration in DNs. Then, to make full use of the ST features and correlations in DNs, MG-ASTGCN is proposed to extract ST information in multi-time scales. In the end, we adopt DDPG to solve the complex MOO-OPF problem. We can draw several conclusion based on experimental results: (i) Extracting ST correlations in DN plays an essential role in solving the MOO-OPF problem, where the performance of the DRL-based approach degenerate significantly without ST attention mechanism; (ii) Compared with several heuristic algorithms, the proposed DRL-based approach tends to spend less time searching for the optimal operation point. Besides, the adoption of the DRL-based approach improves DN’s stability, which has a shorter response time when facing node faults; (iii) In DN graphs, node pairs with more generator access seem to have a stronger spatial correlation. Moreover, in the temporal view, we can conclude that the latest 10 feature vectors of nodes in DN contain more valuable temporal correlation information; (iv) Finding OPF and dealing with technical problems seems to be a trade-off, since our experimental results indicate that overemphasizing voltage fluctuation control results in sub-optimal operations.

In our future work, designing a suitable incentive mechanism to accommodate more RERs will be studied. Moreover, we will consider how to reduce the heavy computation load for training the proposed DRL-based approach.

## REFERENCES

- [1] M. H. Rehmani, M. Reisslein, A. Rachedi, M. Erol-Kantarci, and M. Radenkovic, "Integrating renewable energy resources into the smart grid: Recent developments in information and communication technologies," *IEEE Transactions on Industrial Informatics*, vol. 14, pp. 2814–2825, 7 2018.
- [2] L. Ranalder, H. Busch, T. Hansen, M. Brommer, T. Couture, D. Gibb, F. Guerra, J. Nana, Y. Reddy, J. Sawin, K. Seyboth, and F. Sverrisson, *Renewables in Cities 2021 Global Status Report*. REN21 Secretariat, Mar. 2021.
- [3] S. S. Reddy, "Optimal power flow with renewable energy resources including storage," *Electrical Engineering*, vol. 99, pp. 685–695, 6 2017.
- [4] S. Impram, S. Varbak Nese, and B. Oral, "Challenges of renewable energy penetration on power system flexibility: A survey," *Energy Strategy Reviews*, vol. 31, p. 100539, 2020.
- [5] M. I. Henderson, D. Novosel, and M. L. Crow, "Electric power grid modernization trends, challenges, and opportunities," 2017.
- [6] G. M. Shafiqullah, A. M. T. Oo, D. Jarvis, A. B. M. S. Ali, and P. Wolfs, "Potential challenges: Integrating renewable energy with the smart grid," in *2010 20th Australasian Universities Power Engineering Conference*, 2010, pp. 1–6.
- [7] J. Carpentier, "Optimal power flows," *International Journal of Electrical Power & Energy Systems*, vol. 1, no. 1, pp. 3–15, 1979.
- [8] B. Li, W. Wang, Y. Liu, B. Li, and W. Wen, "Research on power flow calculation method of true bipolar vsc-hvdc grids with different operation modes and control strategies," *International Journal of Electrical Power & Energy Systems*, vol. 126, p. 106558, 03 2021.
- [9] I. U. Khan, N. Javaid, K. A. Gamage, C. J. Taylor, S. Baig, and X. Ma, "Heuristic algorithm based optimal power flow model incorporating stochastic renewable energy sources," *IEEE Access*, vol. 8, pp. 148 622–148 643, 2020.
- [10] K. Nusair and L. Alhmod, "Application of equilibrium optimizer algorithm for optimal power flow with high penetration of renewable energy," *Energies*, vol. 13, 11 2020.
- [11] K. Nusair and F. Alasali, "Optimal power flow management system for a power network with stochastic renewable energy resources using golden ratio optimization method," *Energies*, vol. 13, 7 2020.
- [12] N. Karthik, A. K. Parvathy, R. Arul, and K. Padmanathan, "Multi-objective optimal power flow using a new heuristic optimization algorithm with the incorporation of renewable energy sources," *International Journal of Energy and Environmental Engineering*, vol. 12, no. 4, pp. 641–678, Dec 2021.
- [13] P. Siano, C. Cecati, H. Yu, and J. Kolbusz, "Real time operation of smart grids via fen networks and optimal power flow," *IEEE Transactions on Industrial Informatics*, vol. 8, pp. 944–952, 2012.
- [14] S. , P. Aristidou, and G. Hug, "Data-driven local control design for active distribution grids using off-line optimal power flow and machine learning techniques," *IEEE Transactions on Smart Grid*, vol. 10, no. 6, pp. 6461–6471, 2019.
- [15] X. Lei, Z. Yang, J. Yu, J. Zhao, Q. Gao, and H. Yu, "Data-driven optimal power flow: A physics-informed machine learning approach," *IEEE Transactions on Power Systems*, vol. 36, pp. 346–354, 1 2021.
- [16] R. S. Sutton and A. G. Barto, *Reinforcement Learning: An Introduction*. Cambridge, MA, USA: A Bradford Book, 2018.
- [17] X. Chen, C. Wu, T. Chen, Z. Liu, H. Zhang, M. Bennis, H. Liu, and Y. Ji, "Information freshness-aware task offloading in air-ground integrated edge computing systems," *IEEE Journal on Selected Areas in Communications*, 2021.
- [18] A. Vaswani, N. Shazeer, N. Parmar, J. Uszkoreit, L. Jones, A. N. Gomez, L. u. Kaiser, and I. Polosukhin, "Attention is all you need," in *Advances in Neural Information Processing Systems*, I. Guyon, U. V. Luxburg, S. Bengio, H. Wallach, R. Fergus, S. Vishwanathan, and R. Garnett, Eds., vol. 30. Curran Associates, Inc., 2017.
- [19] B. Yu, H. Yin, and Z. Zhu, "Spatio-temporal graph convolutional neural network: A deep learning framework for traffic forecasting," *CoRR*, vol. abs/1709.04875, 2017.
- [20] P. Veličković, G. Cucurull, A. Casanova, A. Romero, P. Liò, and Y. Bengio, "Graph attention networks," *6th International Conference on Learning Representations*, 2017.
- [21] S. Guo, Y. Lin, N. Feng, C. Song, and H. Wan, "Attention based spatial-temporal graph convolutional networks for traffic flow forecasting," *Proceedings of the AAAI Conference on Artificial Intelligence*, vol. 33, no. 01, pp. 922–929, Jul. 2019.
- [22] Z. Yan and Y. Xu, "Real-time optimal power flow: A lagrangian based deep reinforcement learning approach," *IEEE Transactions on Power Systems*, vol. 35, pp. 3270–3273, 7 2020.
- [23] H. Bouchekara, A. Chaib, M. Abido, and R. El-Sehiemy, "Optimal power flow using an improved colliding bodies optimization algorithm," *Applied Soft Computing*, vol. 42, pp. 119–131, 05 2016.
- [24] P. P. Biswas, P. N. Suganthan, and G. A. Amaratunga, "Optimal power flow solutions incorporating stochastic wind and solar power," vol. 148, pp. 1194–1207, 2017.
- [25] A. Panda and M. Tripathy, "Security constrained optimal power flow solution of wind-thermal generation system using modified bacteria foraging algorithm," *Energy*, vol. 93, pp. 816–827, 12 2015.
- [26] L. Shi, C. Wang, L. Yao, Y. Ni, and M. Bazargan, "Optimal power flow solution incorporating wind power," *IEEE Systems Journal*, vol. 6, no. 2, pp. 233–241, 2012.
- [27] J. D. D. Glover and M. S. Sarma, *Power System Analysis and Design*, 3rd ed. USA: Brooks/Cole Publishing Co., 2001.
- [28] R. Roy and H. Jadhav, "Optimal power flow solution of power system incorporating stochastic wind power using gbest guided artificial bee colony algorithm," *International Journal of Electrical Power & Energy Systems*, vol. 64, pp. 562–578, 01 2015.
- [29] T. P. Chang, "Investigation on frequency distribution of global radiation using different probability density functions," *International Journal of Applied Science and Engineering*, vol. 8, pp. 99–107, 2010.
- [30] S. S. Reddy and P. Bijwe, "Real time economic dispatch considering renewable energy resources," *Renewable Energy*, vol. 83, pp. 1215–1226, 2015.
- [31] S. Zhang, H. Tong, J. Xu, and R. Maciejewski, "Graph convolutional networks: a comprehensive review," *Computational Social Networks*, vol. 6, no. 1, p. 11, Nov 2019.
- [32] Z. Zhu, W. Wu, W. Zou, and J. Yan, "End-to-end flow correlation tracking with spatial-temporal attention," in *Proceedings of the IEEE Conference on Computer Vision and Pattern Recognition (CVPR)*, June 2018.
- [33] X. Shi, H. Qi, Y. Shen, G. Wu, and B. Yin, "A spatial-temporal attention approach for traffic prediction," *IEEE Transactions on Intelligent Transportation Systems*, vol. 22, no. 8, pp. 4909–4918, 2021.
- [34] Y. Chen, L. Zhang, P. Xu, and A. Di Gangi, "Electricity demand response schemes in china: Pilot study and future outlook," *Energy*, vol. 224, p. 120042, 2021.
- [35] Y. Yang, M. Wang, L. Yu, and L. Zhang, "Peak-off-peak load shifting: Are public willing to accept the peak and off-peak time of use electricity price?" *Journal of Cleaner Production*, vol. 199, 06 2018.
- [36] V. Abeykoon, K. Nishadi, R. Senevirathna, P. Ranaweera, and R. Udawapola, "Electricity consumption pattern detection," 01 2016.
- [37] J. Priesmann, L. Nolting, C. Kockel, and A. Praktikno, "Time series of useful energy consumption patterns for energy system modeling," *Scientific Data*, vol. 8, no. 1, p. 148, May 2021.
- [38] I. J. Goodfellow, Y. Bengio, and A. Courville, *Deep Learning*. Cambridge, MA, USA: MIT Press, 2016.
- [39] D. I. Shuman, S. K. Narang, P. Frossard, A. Ortega, and P. Vandergheynst, "The emerging field of signal processing on graphs: Extending high-dimensional data analysis to networks and other irregular domains," *IEEE Signal Processing Magazine*, vol. 30, no. 3, p. 83–98, May 2013.
- [40] C. Wang, B. Samari, and K. Siddiqi, "Local spectral graph convolution for point set feature learning," in *Computer Vision - ECCV 2018 - 15th European Conference, Munich, Germany, September 8-14, 2018, Proceedings, Part IV*, ser. Lecture Notes in Computer Science, V. Ferrari, M. Hebert, C. Sminchisescu, and Y. Weiss, Eds., vol. 11208. Springer, 2018, pp. 56–71.
- [41] S. Mallat, *A Wavelet Tour of Signal Processing, Third Edition: The Sparse Way*, 3rd ed. USA: Academic Press, Inc., 2008.
- [42] M. Simonovsky and N. Komodakis, "Dynamic edge-conditioned filters in convolutional neural networks on graphs," 2017.
- [43] T. P. Lillicrap, J. J. Hunt, A. Pritzel, N. Heess, T. Erez, Y. Tassa, D. Silver, and D. Wierstra, "Continuous control with deep reinforcement learning," 2019.
- [44] D. Cao, W. Hu, X. Xu, Q. Wu, Q. Huang, Z. Chen, and F. Blaabjerg, "Deep reinforcement learning based approach for optimal power flow of distribution networks embedded with renewable energy and storage devices," *Journal of Modern Power Systems and Clean Energy*, vol. 9, pp. 1101–1110, 9 2021.

- [45] M. R. Elkadeem, M. Abd Elaziz, Z. Ullah, S. Wang, and S. W. Sharshir, "Optimal planning of renewable energy-integrated distribution system considering uncertainties," *IEEE Access*, vol. 7, pp. 164 887–164 907, 2019.
- [46] J. Schulman, F. Wolski, P. Dhariwal, A. Radford, and O. Klimov, "Proximal policy optimization algorithms," *CoRR*, vol. abs/1707.06347, 2017.
- [47] Z. Wang, V. Bapst, N. Heess, V. Mnih, R. Munos, K. Kavukcuoglu, and N. de Freitas, "Sample efficient actor-critic with experience replay," *CoRR*, vol. abs/1611.01224, 2016.
- [48] T. Haarnoja, A. Zhou, P. Abbeel, and S. Levine, "Soft actor-critic: Off-policy maximum entropy deep reinforcement learning with a stochastic actor," in *Proceedings of the 35th International Conference on Machine Learning*, ser. Proceedings of Machine Learning Research, vol. 80. PMLR, 10–15 Jul 2018, pp. 1861–1870.
- [49] V. Mnih, A. P. Badia, M. Mirza, A. Graves, T. Lillicrap, T. Harley, D. Silver, and K. Kavukcuoglu, "Asynchronous methods for deep reinforcement learning," in *Proceedings of The 33rd International Conference on Machine Learning*, ser. Proceedings of Machine Learning Research, vol. 48. PMLR, 20–22 Jun 2016, pp. 1928–1937.
- [50] M. A. M. Shaheen, H. M. Hasanien, S. F. Mekhamer, and H. E. A. Talaat, "Optimal power flow of power networks with penetration of renewable energy sources by harris hawks optimization method," in *2020 2nd International Conference on Smart Power Internet Energy Systems (SPIES)*, 2020, pp. 537–542.
- [51] J. A. Bondy and U. S. R. Murty, *Graph Theory with Applications*. New York: Elsevier, 1976.



**Zhi Liu** (S'11-M'14-SM'19) received the Ph.D. degree in informatics in National Institute of Informatics. He is currently an Associate Professor at The University of Electro-Communications. His research interest includes video network transmission and mobile edge computing. He is now an editorial board member of Springer wireless networks and IEEE Open Journal of the Computer Society. He is a senior member of IEEE.



**Hongyang Lai** is majoring in Smart Grid Information Engineering in the University of Electronic Science and Technology of China (UESTC), with a double degree in Finance. He is currently pursuing his Bachelor Degree under the supervision of Professor Weihao Hu. His research interests include application of artificial intelligence in power system, renewable energy system planning and wind power generation.



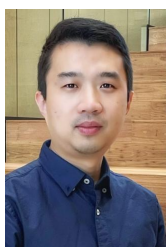
**Jinhao Li** is majoring in Smart Grid Information Engineering in the University of Electronic Science and Technology of China (UESTC), with a double degree in Mathematics. He is currently pursuing his Bachelor Degree under the supervision of Professor Yanru Zhang. Besides, he He is a member of the IntelliGame Laboratory in Big Data Research Centre at UESTC. His main research interests are game theory, machine learning deep learning, and their applications.



**Ruichang Zhang** was born in Ningxia, China, in 1997. He received the B.S. degree in chemistry and obtained a minor certificate in economics from Xiamen University, Fujian, China, in 2019. He is currently a student of the School of Computer Science and Engineering, University of Electronic Science and Technology of China(UESTC). His current interests include machine learning, data mining and game theory.



**Yanru Zhang** (S'13-M'16) received the B.S. degree in electronic engineering from University of Electronic Science and Technology of China (UESTC) in 2012, and the Ph.D. degree from the Department of Electrical and Computer Engineering, University of Houston (UH) in 2016. She is now working as the Postdoctoral Fellow at Chinese University of Hong Kong. Her current research involves the contract theory and matching theory in network economics, Internet and applications, wireless communications and networking. She received the best paper award at IEEE ICC 2017 and ICCS 2016.



**Hao Wang** (M'16) received the Ph.D. degree from the Chinese University of Hong Kong in 2016. He was a Postdoctoral Research Fellow with Stanford University and a Washington Research Foundation Innovation Fellow with the University of Washington. He is currently a Lecturer with the Department of Data Science and Artificial Intelligence, Faculty of Information Technology, Monash University, Australia. His research interests are in optimization, machine learning, and data analytics for power and energy systems. More information at